國 立 交 通 大 學

機械工程學系

碩士論文

以微機電製程製作微型質子交換膜燃料電池之實驗研究

The Experimental Study on Micro PEMFC Manufactured by Using MEMS Technology

研 究 生：鄭致瑋

指導教授：陳俊勳　教授

中 華 民 國 九十八 年 六 月

以微機電製程製作微型質子交換膜燃料電池之實驗研究

The Experimental Study on Micro PEMFC Manufactured by Using MEMS Technology

研究生：鄭致瑋　　Student： Chih-Wei Cheng

指導教授：陳俊勳　　Advisor：Chiun-Hsun Chen

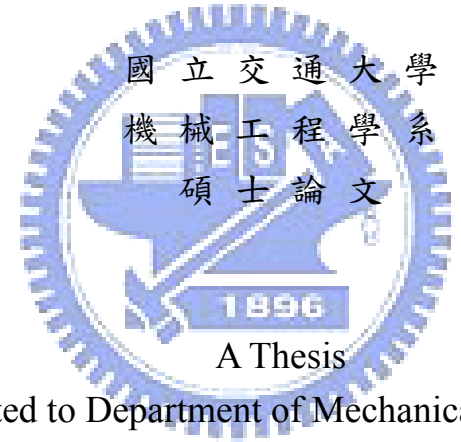

國立交通大學

機械工程學系

碩士論文

A Thesis

Submitted to Department of Mechanical Engineering

College of Engineering

National Chiao Tung University

In Partial Fulfiillment of the Requirements

For the Degree of

Master of Science

In Mechanical Engineering

June 2009

Hsinchu, Taiwan, Republic of China

中華民國九十八年六月

The Experimental Study on Micro PEMFC Manufactured by Using MEMS Technology

以微機電製程製作微型質子交換膜燃料電池之實驗研究

學 生:鄭 致 瑋　　指 導 教 授:陳 俊 勳

國立交通大學機械工程學系

摘要

本文主要是研究以微機電製程製作微型質子交換膜燃料電池之實驗研究。探討反應面積為 2 公分x2 公分的單電池。本論文實驗分成兩大部份，一部份是實驗參數測試，另一部份是耐久度測試。實驗參數包括氣體再熱溫度、集電片材料影響、雙極板開孔率影響與陰極氣體比較。

由實驗結果可知，集電片的導電面積與材料對於電池性能有顯著的影響，尤其是前者; 對於增加反應氣體的再熱溫度，微型燃料電池增加的性能有限;雙極板開孔率 75%相較於開孔率為 50%與 67%有最佳的性能曲線;增加陰極氣體空氣的流量，可以改善高電流情況下的濃度極化現象，所以若我們能增加氣體擴散層的擴散能力，則可以減少兩者的性能差距。此外，長時間的測試下，在固定電壓 0.4V 且長達 10 小時的耐久度測試後，本實驗所組成的微型質子交換膜燃料電池，測試的性能差距在±2.2%以內。

Student: Chih-Wei Cheng Advisor: Prof. Chiun-Hsun Chen

Institute of Mechanical Engineering

National Chiao Tung University

ABSTRACT

This study fabricates micro PEMFC (Proton Exchange Membrane Fuel Cell) by using the MEMS (Micro Electro Mechanical Systems) technology. The active area of the membrane is 2cm×2cm. The study is divided into two categories; one is the parametric experimental investigation, and the other is the durability test. In experimental works, the parameters include reheat temperature, material of current collector slices, open ratio and different cathode gases, respectively.

According to the experimental results, both the conducting area and material of current collector slices have great influence on the performance of micro PEMFC, especially the former one. The increment of cell's performance is finite by increasing the gas reheats temperature. The performance is better for open ratio 75% compared with 50% and 67%. The concentration polarization is improved by increasing the air flow rate at high current density and if the GDL diffusive capability in the latter cell could be promoted, the differences between these two cells' performances would be reduced. Furthermore, the performance deviation at fixed operating voltage 0.4V is less than ±2.2%.

ACKNOWLEDGEMENTS

在碩士的生活中，藉由不同領域的研究，我深深體會如何對於問題應變與解決能力的重要性。由衷地感謝　陳俊勳教授　對我耐心的指導，培養我獨立思考的能力，才能有此份論文的成果，使我感覺到現在自己與兩年前的我有所茁壯與成長。

同時要特別感謝元智大學　翁芳柏副教授與工研院能環所　曹芳海組長於口試期間給予的指正與建議，使得本論文更加完善。

在兩年的研究生涯中，非常感謝文耀、竣翔、振忠、彥成、遠達、維義、成陽、家維、瑭原、榮貴、耀文、仁浩與NDL的哲魁等學長在生活與研究上的指導。同時一起畢業的振稼、智欽、金輝、育祈，這兩年有你們的陪伴，讓我有個難忘的碩士生涯，還有瑋琮、義嘉、信錡、長新等學弟幫助我處理些繁雜瑣事，讓我順利地完成本論文。

同時也感謝機械系足的夥伴們，在研究之餘，可以一同在足球場上拼戰，抒發一些壓力，成為我前進的動力。

最後，將這份榮耀給我摯愛的家人，感謝生我、育我的爸爸、媽媽以及大哥、二哥與三姊，感謝你們在這段期間對我一路的支持與鼓勵，讓我在生活上無後顧之憂。

CONTENTS

ABSTRACT (CHINESE) i

ABSTRACT (ENGLISH) ii

ACKNOWLEDGEMENTS iii

CONTENTS iv

LISTS OF TABLES vii

LISTS OF FIGURES ix

NOMENCLATURE xii

Chapter 1 1

1.1 Motivation and Background 1

1.2 Literature Review 3

1.3 Scope of Present Study 7

Chapter 2 13

2.1 History of Fuel Cell 13

2.2 Principle of the Fuel Cell 14

2.2.1 Thermodynamics 14

2.2.2 Kinetics 15

2.3 Type of Fuel Cells 19

2.3.1 SOFC 21

2.3.2 MCFC 21

2.3.3 PAFC 22

2.3.4 AFC 22

2.3.5 PEMFC 22

2.4 Principle of PEMFC 23

2.5 Structure of PEMFC 24

2.5.1 Bipolar Plate 24
2.5.2 Gas Diffusion Layer (GDL) 24
2.5.3 Gasket 24
2.5.4 Proton Exchange Membrane (PEM) 25
2.5.5 Active Layer 25
Chapter 3 28
3.1 Processes of Fabricating the Flow Field Plates 28
3.1.1 Mask Design 28
3.1.2 RCA Clean 28
3.1.3 Deposition the Block Layer Si_3N_4 31
3.1.4 Fabrication of Photolithography 31
3.1.5 Removing the Block Layer 33
3.1.6 Etching the Si by KOH 33
3.1.7 Removing the Block Layer (Si_3N_4) 33
3.2 Assembly and Components of micro PEMFC 34
3.2.1 Components of Micro PEMFC 34
3.2.2 Assembly of Micro PEMFC 34
3.2.3 Three Type Current Collector Slices 34
3.2.4 Assembly of Air-Breathing Micro PEMFC 35
3.3 Test Station 35
3.4 Uncertainty Analysis 37
3.4.1 Analyses of the Propagation of Uncertainty in Calculations 38
3.4.2 The Uncertainty of Test Station Apparatus 39
3.4.3 The Uncertainty of Fuel Cell Power Density 43
Chapter 4 54
4.1 Reference Case 54

4.2 The Influences of Current Collector Material and Conducting Area 56
4.3 The Influences of Gas Reheat Temperature 58
4.4 The Influence of Bipolar Plate Open Ratio in Anode and Cathode 60
4.5 The Comparison of Three Cathode Gases With and Without Flow Channel 62
4.6 Durability Test of micro PEMFC 64
Chapter 5 74
Conclusions and Recommendations 74
5.1 Conclusions 74
5.2 Recommendations 75
Reference 76
APPENDIX A 79

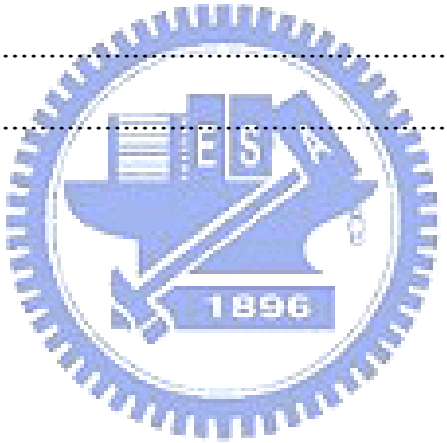

LISTS OF TABLES

Table 2.1 The Five Major Types of Fuel Cells 20

Table 3.1 the Steps of RCA Clean Process 30

Table 3.2 Parameter of Track MK-8 32

Table 3.3 Instrument of Hardware Specifications 36

Table 3.4 Function of Software 37

Table 3.5 One or More PEMFC Testing Range 37

Table 3.6 Uncertainty of Electronic Load Potential Meter 39

Table 3.7 Uncertainty of Electronic Load Current Meter 40

Table 3.8 Uncertainty of Anode MFC 41

Table 3.9 Uncertainty of Cathode MFC 41

Table 3.10 Uncertainty of Air Bleeding MFC 41

Table 3.11 Uncertainty of Anode Temperature Controller 42

Table 3.12 Uncertainty of Cathode Temperature Controller 42

Table 3.13 Uncertainty of Cell Temperature Controller 43

Table 3.14 The Measuring Uncertainty of Fuel Cell 43

Table 4.1 The Properties of MEA 54

Table 4.2 Testing Conditions of Reference case 55

Table 4.3 The experimental results of Reference Case 56

Table 4.4 The Best Performance for three current collector slice materials 57

Table 4.5 The result comparison of reheat temperatures, 25^0C, 60^0C, and 90^0C of pure O_2 oxidizer (by flow field) 59

Table 4.6 The result comparison of reheat temperatures, 25^0C, 60^0C, and 90^0C for Air-breathing cell 60

Table 4.7 Dimension of Flow Field Plate 60

Table 4.8 The best performance of three open ratios 50%, 67% and 75%61
Table 4.9 The Comparison of Three Cases Cathode Gas 63

LISTS OF FIGURES

Fig. 1-1 The Petroleum's Price in Recent Year 8

Fig. 1-2 Portable Power Sources, Ranged from KW to W 8

Fig. 1-3 (a) Bipolar Plate Design and (b) Monolithic Design [2] 9

Fig. 1-4 Comparison of Power Densities for Bilayer and Monolithic Design [2] 9

Fig. 1-5 Depiction of an Assembled Fuel Cell in PCB Design and Components [11-12] 10

Fig. 1-6 Depiction of the Cathodes Plates for the Three Opening ratios (cell geometries I–III) [13] 10

Fig. 1-7 Design of Cathode Current Collectors with Different Open Area: (a) 92%, (b) 77%, (c) 64% and (d) 52% [14] 11

Fig. 1-8 Under-Rib Convection and Transport in Serpentine Flow-Field: (a) Definition of Path-Length, z; (b) Under-Rib Convection and Transport Mechanisms [16]. 11

Fig. 1-9 Construction of Basic Parallel Flow-Fields: (a) Basic Multi-Pass Channel Patterns; (b) Parallel Arrangement of 3-Pass Channel Patterns [16]. 12

Fig. 1-10 (a) New Bio-Inspired Leaf Flow Pattern. (b) New Bio-Inspired Lung Flow Pattern [17]. 12

Fig. 2.1 a Typical I-V Curve For a PEMFC 26

Fig. 2.2 I-V Curve of Fuel Cell 26

Fig. 2.3 The Linear Drop in the Middle of the I-V Curve 27

Fig. 2.4 Sandwich Structure of PEMFC 27

Fig 3.1 The Flow Charts of Flow Field Plate Fabrication 44

Fig. 3.2 Open Ratio (a) 50% (b) 67% (c) 75% 45

Fig. 3.3 Wet Bench 45
Fig. 3.4 Spin Drying 46
Fig. 3.5 PECVD & ICP 46
Fig. 3.6 Track MK-8 47
Fig. 3.7 Patterns of Flow Field Plates 47
Fig. 3.8 Acrylic Plate 48
Fig. 3.9 Flow Field Plates 48
Fig. 3.10 Current Collector Slices 49
Fig. 3.11 GDL and MEA 49
Fig. 3.12 The Steps of Assembly Micro PEMFC 50
Fig. 3.13 The Assembly of Micro PEMFC 50
Fig. 3.14 Three Type Current Collector Slices 51
Fig. 3.15 Assembly of Air-Breathing Micro PEMFC 51
Fig. 3.16 Test Station 52
Fig. 3.17 Test of a Single micro PEMFC 52
Fig. 3.18 Components of Test Station 53
Fig. 4.1 Performance Curve of Reference Case 65
Fig. 4.2 Three Cases Current Collector slice (a) two narrow strips (b) Cu square (c) Cu/Au square 65
Fig. 4.3 The Performance Curve of Three Different Current Collectors . 66
Fig. 4.4 The Average Moving Distance of Electron 67
Fig. 4.5 I-V Curve of Three Reheat temperatures in O_2 (by flow field) .. 67
Fig. 4.6 I-P Curve of Three Reheat Temperatures in O_2 (by flow field) .. 68
Fig. 4.7 I-V Curve of Three Reheat Temperature in Air-breathing 68
Fig. 4.8 I-P Curve of Three Reheat Temperatures in Air-breathing 69
Fig. 4.9 The Performance Curve of three Open Ratios 70

Fig. 4.10 I-V Curve at Air Flow Rate 30sccm 71
Fig. 4.11 I-V Curve at Air Flow Rate 150sccm 71
Fig. 4.12 The Performance Curve of Three Cases Cathode Gas 72
Fig. 4.13 Instability Area and Deviation Analysis of Durability Test 73

NOMENCLATURE

C	Reactant molar concentration (kmol/m^3)
C_{ref}	Reference molar concentration (kmol/m^3)
C_C^R	Reactant molar concentration of hydrogen in flow channel (kmol/m^3)
C_L^R	Reactant molar concentration of hydrogen in catalyst layer (kmol/m^3)
D_{eff}	Gas effective diffusivity (m^2/s)
D	Effective mass diffusion coefficient (m^2/s)
F	Faraday constant (C/kmol)
H_C	Flow channel height (m)
H_G	GDL height (m)
h	Gas enthalpy (J/kg)
i	Current density vector
J	Diffusive flux
J_C^{conv}	The mass flow rate from flow channel to GDL (kg/s)
J_G^{diff}	The mass flow rate from GDL to catalyst layer (kg/s)
j	Transfer current density (A/m^2)
j_e	Exchange current density (A/m^2)
M	Mixture molecular weight (kg/kmol)
N	Superficial flux (kmol/m^2·s)
n	Number of species, or number of electrons participating in a reaction
p	Absolute pressure (Pa)
q	Heat flux (J/m^2)
R	Universal gas constant (8.3143 kJ/kmol·K)
S	Reaction surface area (m^2)
Sh	Sherwood number

T	Absolute temperature (K)
U	Fluid velocity vector (m/s)
u	Thermodynamic equilibrium potential (V)
V	Medium volume (m^3)
v	Pore-water velocity in membrane (m/s)
x	Mole fraction
Y	Mass fraction
z	Charge number

Greek symbols

α	Mass transfer coefficient
β	kinetic constant
ε	Porosity
ρ	Fluid density (kg/m^3)
η	Over-potential (V)
κ	Permeability (m^2)
μ	Dynamic viscosity (kg/m·s)
σ	Electrical conductivity (1/Ω·m)
τ	Shear stress tensor (N/m^2)
δ	Tortuosity
φ	Concentration exponent
$\dot{\omega}$	Mass production rate in gas phase ($kg/m^3 \cdot s$)
Φ	Potential (V)

Superscripts

conv	Convection

diff	Diffusion
K	Reaction kinetics
N	Nerst
R	Molar
tot	Total

Subscripts

an	Anode
C	Flow channel
ca	Cathode
con	Concentration loss
e	Exchange
eff	Effective value
G	Gas diffusion layer
in	Inlet
L	Catalyst layer

Chapter 1

Introduction

1.1 Motivation and Background

Since industrial revolution, fossil fuel has been used so excessively that the amounts of green-house gases, such as CO_2, CH_4, and N_2O, etc., become more and more in the atmosphere. Many countries, especially China and India, are developing excessively that makes the green-house effect being more serious. Combining with the fact that the petroleum's price has been soared due to the depletion in recent years; see Fig. 1-1, mankind is facing a crucial issue that is to look for the alternative energy resources, which must avoid arising the questions of green-house effects. In other words, the new energy resource or technology should be effective, efficient, and more environmental friendly to replace the traditional internal combustion engine.

In recent years, many countries have been devoted to developing the alternative power sources, including nuclear, bio, solar, hydrogen, and wind energies. Fuel cell is one of these developing power sources, because of its high electrochemical performance efficiency, simple stacks design, pollution-free, noise-free and low temperature operation. Therefore, the fuel cell is expected to be the mainstream of green energy science and technology in 21st century.

The fuel cell is a quite promising energy technology that has been applied extensively in recent years. The proton exchange membrane fuel

cell (PEMFC) is the common-used one due to its relatively low operation temperature. For an example, PEMFC has become a promising candidate for portable power sources, ranged from KW to W; see Fig. 1-2. According to fuel type, PEMFC can divide into two major categories, the hydrogen and methanol. Hydrogen-oxygen PEMFC has higher Open Circuit Voltage (OCV) than that of methanol one, which there are some drawbacks. For examples, methanol itself can be harmful to people, it also generates mixed potential to lower performance, the produced CO can poison Pt catalyst, and etc. At present, the reduction of CO_2 emission becomes a seriously problem. The product of hydrogen-oxygen PEMFC is the water only, whereas methanol one can produce CO_2, therefore, the application of hydrogen fuel in PEMFC is preferred.

Different from the internal combustion engine, fuel cell is not limited by the Carnot cycle, so its energy transformation can be up to 60~80%. The hydrogen-oxygen fuel cell transfers the gases, such as hydrogen and oxygen, to the fuel cell's anode and cathode electrodes, respectively. Then, the hydrogen is catalyzed by the catalyst, Pt, and the product, hydrogen ion, reacts with the oxygen to generate electricity and water by the electrochemistry reactions, which are described as follows:

$$\text{Anode: } H_2 \xrightarrow{Pt} 2H^+ + 2e^- \tag{1.1}$$

$$\text{Cathode: } \frac{1}{2}O_2 + 2H^+ + 2e^- \rightarrow H_2O + Heat \tag{1.2}$$

$$\text{Overall: } H_2 + \frac{1}{2}O_2 \rightarrow H_2O + Heat \tag{1.3}$$

The power generation of conventional fuel cell is in the order of Kilowatt, which is too great for 3C commercial products, such as cellular phone, lap-top, etc., which need no more than 10W. Therefore, the

micro-fuel cell becomes an important research topic now. In addition, Taiwan has been devoted to developing the semiconductor industry in recent years, so the technologies of semiconductor fabrications become more mature than ever before. Therefore, this work intends to fabricate the micro fuel cell by the MEMS (Micro Electro Mechanical Systems) technology that can lower the size and cost of fuel cell. More than that, it also enables to increase the generated power per unit volume.

1.2 Literature Review

The flow field structures in fuel cells have to meet several requirements, such as homogeneous fluid distribution, product water removal, good current transport, good under-rib convection and high conductivity. Each factor can considerably influence the performance of fuel cells. However, this work, as mentioned previously, is focused on the effects of flow field structure in micro PEMFC.

Yu et al. [1] designed and fabricated the micro flow channels by using MEMS techniques, including photolithography, dry and wet etching, and chemical and physical vapor deposition. The material of wafer base was silicon. This paper's primary research was to deposit Cu/Au composite layers in different thickness on the top of silicon wafer, including 0.5μmAu, 1.4μm Cu&0.2μm Au, and 1.5μm Cu&0.9μm Au. The composite layers were primarily to reduce their resistance as the current collectors. The results indicated that the cell performance is improved by increasing the thickness of the composite layer on the silicon wafer.

Meyers and Maynard [2] also fabricated the micro flow channels by using MEMS techniques. The wafer base was silicon. Fig. 1-3 illustrates (a) the bipolar plate design and (b) the monolithic design. This research was primarily to compare bipolar and monolithic designs. Bipolar design is similar to the standard cell sandwich commonly used in PEMFC system, and monolithic design is essentially an "unfolded" fuel cell with the anode and cathode on the same substrate. The experimental results were that bipolar design's performance was better than that of monolithic one, see Fig. 1-4. The research also suggested that many system-level issues, like thermal management, air movement, fuel delivery, humidification control, water management, power load management, and system integration, must be considered in order to achieve higher performance.

Lee and Chuang [3] employed porous silicon as a gas diffusion layer (GDL) to minimize a micro-fuel cell. Pt catalyst was deposited on the surface of the porous silicon by physical vapor deposition (PVD) method to improve the porous silicon conductivity. Porous silicon with Pt catalyst replaced traditional GDL, and the Pt metal, remaining on the rib, was used to form a micro-thermal sensor in single lithographic process.

The researches of [4] and [5] had focused on measuring important data on the effect of cell temperature, fuel temperature, fuel humidity and other key factors on cell performance.

Nguyen and White [6] showed that the potential loss caused by the membrane contributes to a large proportion of the total loss of fuel cell stacks. In order to reduce this loss, reactants at the anode must be humidified. As for the cathode, if air, instead of pure oxygen, is used,

humidification is also needed.

For the studies for micro PEMFC and DMFC, the MEMS technology and Si-based substrate have been widely used. For examples, Kelley et al. [7], Shah et al. [8], Cha et al. [9], and Lu et al. [10] all fabricated flow field structures using Si wafers.

Schmitz et al. [11, 12] successfully designed a planar fuel cell that was primarily made by the print circuit board (PCB) as materials, see Fig. 1-5. The PCB is a new base of bipolar plate which can be used in MEMS technology. They operated the air-breathing fuel cell in the atmosphere, and the power density could reach to 110mW/cm^2 in 0.5V.

Schmitz et al. [13] researched the air-breathing fuel cells under the influence of different opening area ratios, which are 33%, 50% and 80%, respectively; see Fig.1-6. They were operated in the room temperature, and it was found that the case of area ratio 80% has the best performance for the water management.

Jeong et al. [14] also proofed the influence on air-breathing PEMFCs by using four kinds of cathode opening area ratio; see Fig.1-7. At low current density, the power density decrease with increasing the opening ratio. But at the high current density, the level of the power density is in successive order, that is 77%>64%>92%>52%. The opening ratio of 64% will reach the concentration polarization first comparing to that of 92%. And at low current density, the power density will increase with the surrounding humidity, but such trend does not appear at high current density.

Cha et al. [15] covered the investigation range of flow channels from macro feature size (>500μm) to micro feature size (<100μm). Each

flow pattern archetype exhibits unique scaling behavior. For most flow pattern archetypes, optimal feature size occurs at an intermediate channel dimension. Extremely small flow channels do not optimize performance despite improved mass transport. Pressure drop loss and flow travel path in the cathode compartment are the major factors to determine the optimal size. The scaling phenomena are explained in conjunction with the details of oxygen distribution in the cathode flow channels and gas diffusion layer.

Jin et al. [16] indicated that the flow-field for reactant distribution is an important design factor that influences the performance of PEMFCs. They focused on increasing the path-length difference, Δz, in serpentine flow-fields with the hypothesis that an enhancement of under-rib convection between neighboring channels improved the performance of PEMFCs as illustrated in Figs. 1-8 and 1-9. The resultant maximum path-length difference between neighboring flow-channels is expected to enhance under-rib convection and transport, thereby improving the performance. In addition, the highly-interlaced channel patterns in Multi-Pass Serpentine Flow-Fields (MPSFFs) are expected to improve the uniformity of local conditions, such as reactant and product concentrations, temperature and liquid water saturation in the active cell area.

Jason et al. [17] showed that PEMFC performance is directly related to the flow channel design on bipolar plates. Power gains can be found by varying the type, size, or arrangement of channels. This study presented two new flow channel patterns: a leaf design and a lung design; see Fig.1-10. These bio-inspired designs combine the advantages of the

existing serpentine and interdigitated patterns with inspiration from patterns found in nature. This research showed promising results for bio-inspired flow patterns with noticeable improvement in pressure loss, overall performance, and peak power density. For the new leaf and lung designs, the optimum operating conditions are found as 65~75^{0}C cell temperature, 2-atm backpressure, and 100% relative humidity.

1.3 Scope of Present Study

This thesis fabricates the single micro PEMFC by using the MEMS technology. The pattern designed by AutoCAD is manufactured on the bipolar plates by using several work stations, such as wet bench, plasma-enhanced chemical vapor deposition (PECVD), and Track MK-8. After that, the single micro PEMFC is assembled by bipolar plates, acrylic plates, current collector slices and membrane-electrode-assembly (MEA). Finally, a series of performance experiments on a single micro PEMFC are carried out and demonstrated in this work.

The experimental parameters include reheat temperature, material of current collector slices, open ratio, air-breathing, and cathode gas, respectively. According to above performance experimental results, the optimal parameters of the single micro PEMFC can be identified. Furthermore, this work also investigates the durability of such cell that is tested at fixed operating voltage for 10 hours.

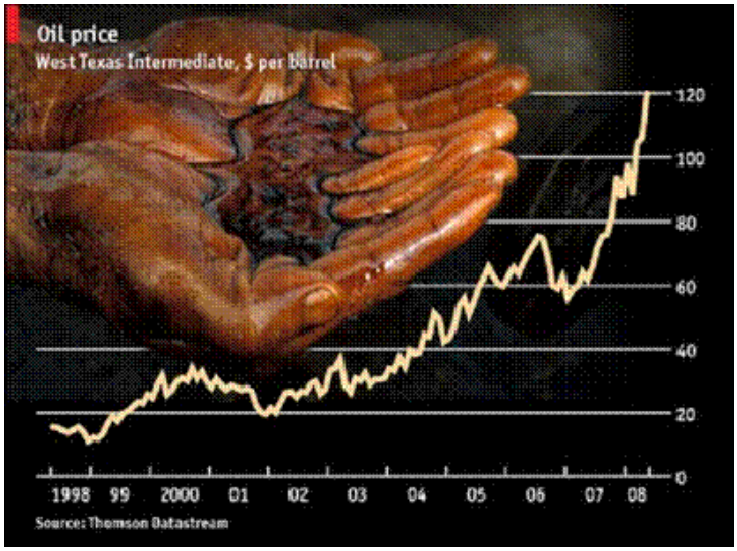

Fig. 1-1 The Petroleum's Price in Recent Year

http://blog.roodo.com/2008_visionary/archives/cat_521131.html

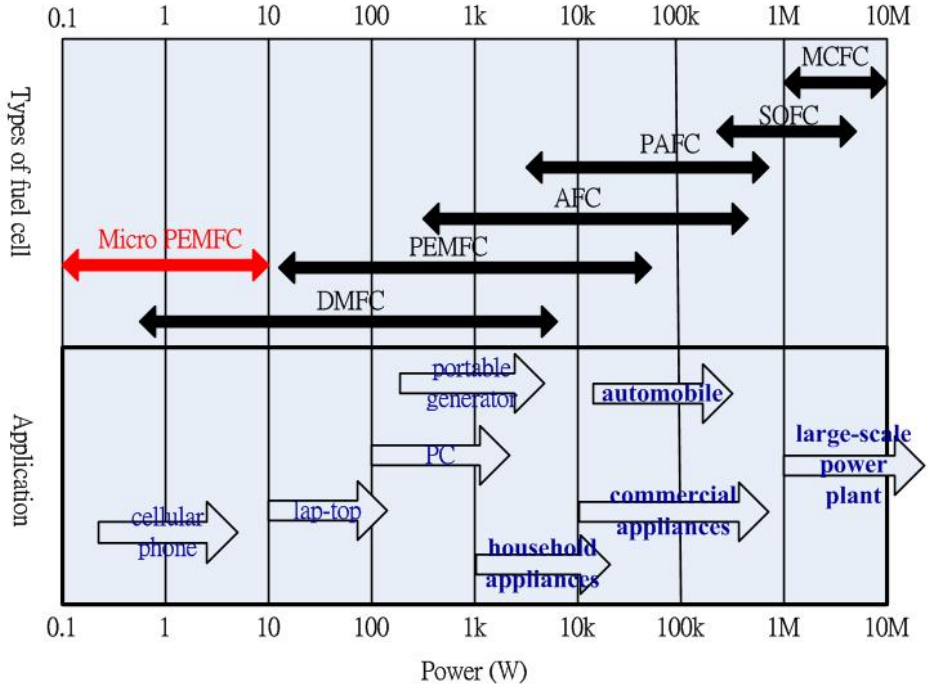

Fig. 1-2 Portable Power Sources, Ranged from KW to W

http://www.nhu.edu.tw/~society/e-j/63/63-32.htm

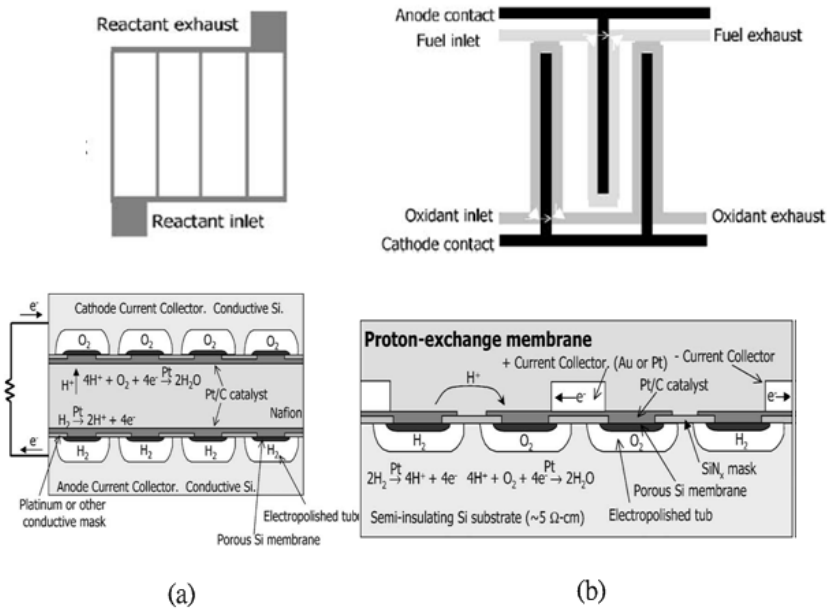

Fig. 1-3 (a) Bipolar Plate Design and (b) Monolithic Design [2]

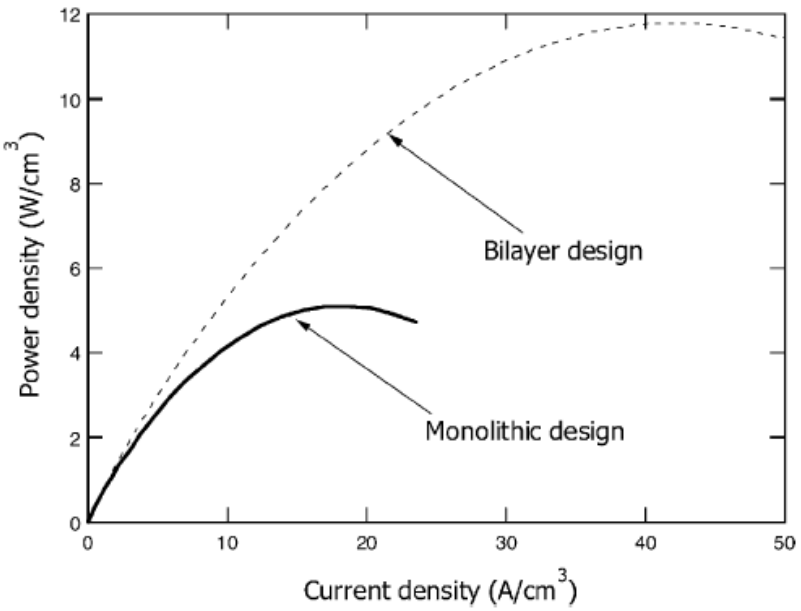

Fig. 1-4 Comparison of Power Densities for Bilayer and Monolithic Design [2]

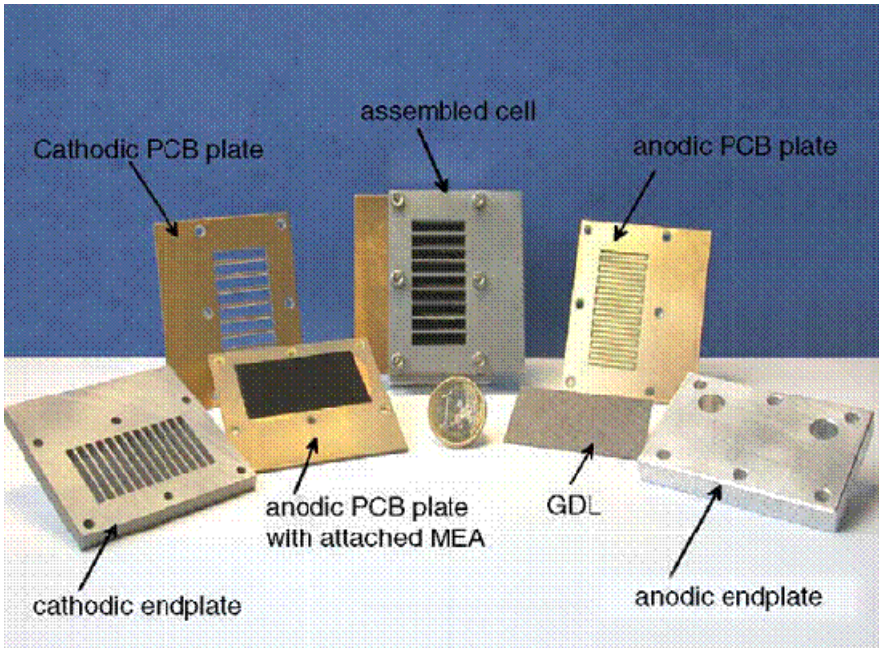

Fig. 1-5 Depiction of an Assembled Fuel Cell in PCB Design and Components [11-12]

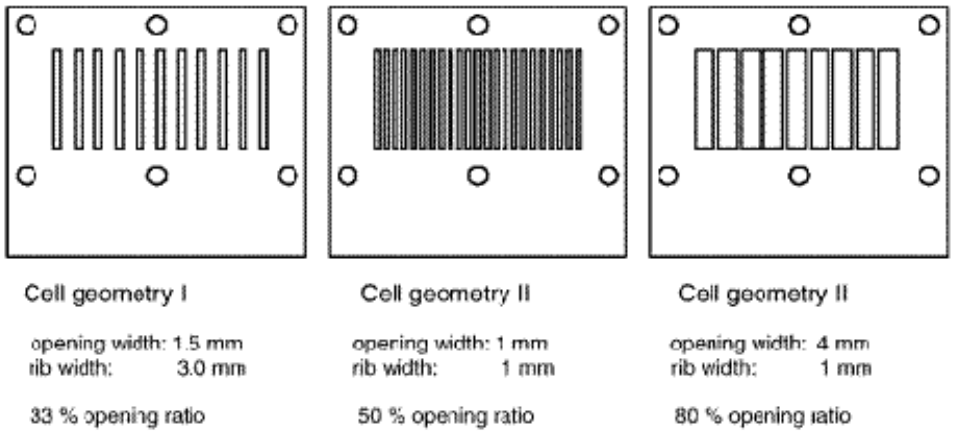

Fig. 1-6 Depiction of the Cathodes Plates for the Three Opening ratios (cell geometries I–III) [13]

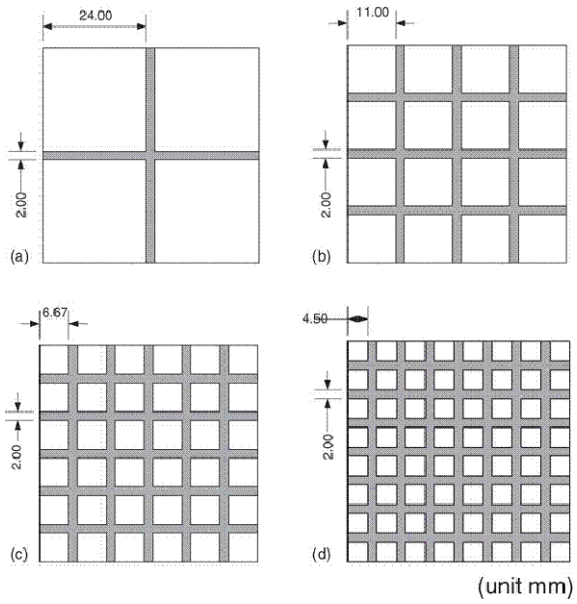

Fig. 1-7 Design of Cathode Current Collectors with Different Open Area: (a) 92%, (b) 77%, (c) 64% and (d) 52% [14]

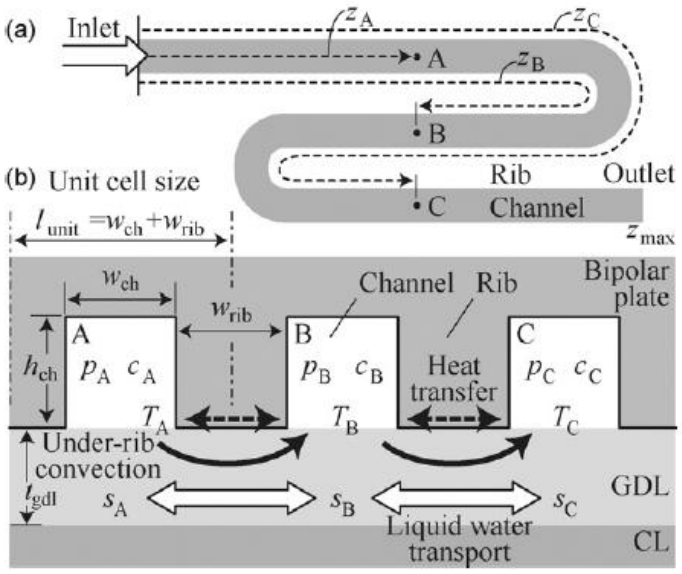

Fig. 1-8 Under-Rib Convection and Transport in Serpentine Flow-Field: (a) Definition of Path-Length, z; (b) Under-Rib Convection and Transport Mechanisms [16].

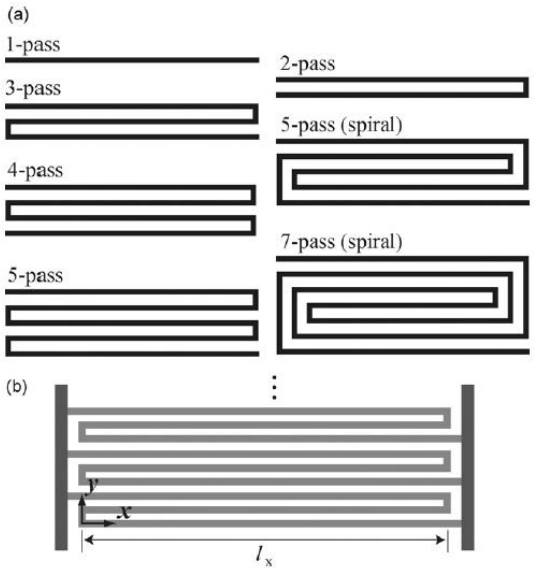

Fig. 1-9 Construction of Basic Parallel Flow-Fields: (a) Basic Multi-Pass Channel Patterns; (b) Parallel Arrangement of 3-Pass Channel Patterns [16].

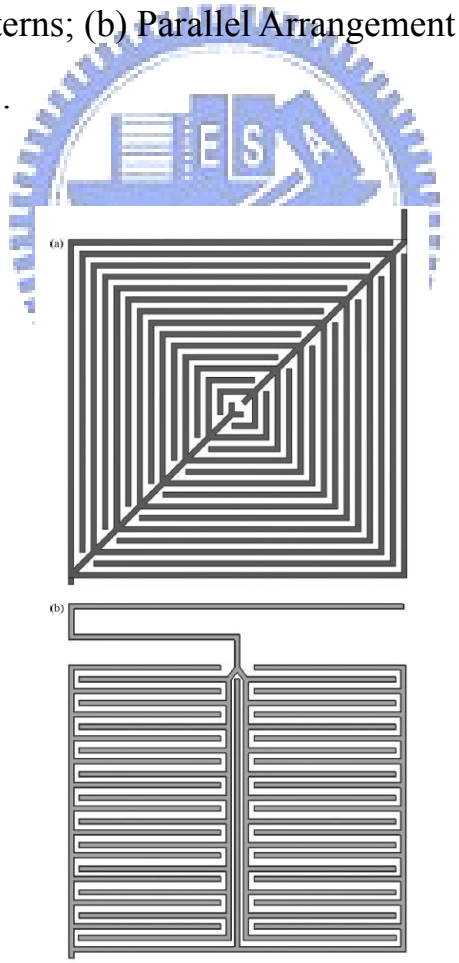

Fig. 1-10 (a) New Bio-Inspired Leaf Flow Pattern. (b) New Bio-Inspired Lung Flow Pattern [17].

Chapter 2

Fundamentals of Fuel Cell

2.1 History of Fuel Cell

In 1839, William Grove discovered the electrolytic reverse reaction of water that could generate the faint current, but the science in technology of catalyst was not fully ripe at that time. So the discovery was not developed, but this principle was an initial concept in history of fuel cell. Until 1889, Mord and Langev utilized precious metal Pt as the catalyst to develop the first cell under the Grove's conception. The cell could generate a current density of 0.2A/cm^2, and then the cell was named as the fuel cell formally.

In 1959, Francis Bacon fabricated a cell stack that could generate 5kW to drive fractional power's tools such as electric saw. But he used alkaline electrolyte and Ni as the catalyst, which was different from one (Pt) used by Mord and Langev. So this application made the technology of fuel cell to go out of the laboratory.

1960~1970, NASA used the fuel cell as the main power source of the space vehicle, because the water produced by fuel cell could supply astronauts to drink in the outer space. From then to now, it has already passed nearly 50 years, but the fuel cell still does not have popularized in commercialization, because the materials and cost of manufacture are so expensive in the past.

In recent years, owing to fast growing development of fabrication of

MEMS (Micro electromechanical Systems) and nanotechnology, the fuel cell can be minimized in the scale. So the application of fuel cell power will be widespread and change the range from KW to W in the future.

2.2 Principle of the Fuel Cell

2.2.1 Thermodynamics

Fuel cell is more efficient than heat engines because it converts chemical energy to electrical energy directly. Carnot cycle shows the possible maximum efficiency of a heat engine, which can be expressed as:

$$\eta = \frac{T_H - T_L}{T_H} \quad (2\text{-}4)$$

where T_H is the maximum temperature and T_L is the rejection temperature of the heat engine. For a typical heat engine that operates at $675K$ and rejects heat at $325k$, the Carnot efficiency limit is 52%.

The ideal efficiency of a fuel cell is given by the ratio of the thermodynamically extractable energy of the reaction to the total heat energy that would have been released by the reaction in combustion:

$$\eta = \frac{\Delta G}{\Delta H} \quad (2\text{-}5)$$

At standard conditions, ΔH^0 for the hydrogen/oxygen reaction is $-285.83KJ/mole$ and ΔG^0 is $-237.14KJ/mole$, giving a theoretical efficiency limit of 83%.

Although ΔG^0 represents the energy potential that can be extracted by a fuel cell at standard condition, this energy is expressed by the fuel cell as an electrical potential, or voltage (E_0):

$$E_0 = \frac{\Delta G^0}{2F} \tag{2-6}$$

At standard conditions, this equation gives $1.23V$, which is referred as the fuel cell open circuit voltage (OCV).

ΔG is a function of temperature and pressure, therefore, the fuel cell open circuit voltage changes depending on the operating conditions. These dependencies are described by the Nernst equation:

$$E_{Nernst} = E_0 + \frac{RT}{2F} ln \frac{P_{H_2} P_{O_2}^{\frac{1}{2}}}{P_{H_2O}} \tag{2-7}$$

The ideal fuel cell voltage decreases with increasing temperature, but usually the opposite trend is true for the actual fuel cell efficiency due to accelerated electrochemical reaction kinetics at higher temperatures.

2.2.2 Kinetics

An ideal fuel cell would supply an infinite current while maintaining the constant voltage determined by the Nernst equation. But in fact, the actual voltage output of a real fuel cell is less than the ideal thermodynamically predicted voltage. Furthermore, the more current is drawn from a real fuel cell, the more the voltage output of the cell declines, limiting the total power that the fuel cell can deliver. The performance of a real fuel cell device can be summarized with a graph of its current versus voltage characteristics. Such graph, called an *I-V* curve, shows the real voltage output of the fuel cell for a given current output. An example of a typical *I-V* curve for a PEMFC is shown in Fig. 2.1.

The voltage output of a real fuel cell is less than the

thermodynamically predicted voltage output due to irreversible kinetic losses. The more current is drawn from the cell, the greater these losses. There are three major types of fuel cell losses, which give a fuel cell *I-V* curve to its characteristic shape as shown in Fig 2.2:

1. Activation losses
2. Ohmic losses
3. Concentration losses

An equation for the true fuel cell *I-V* behavior can thus be written by starting with the thermodynamically predicted voltage output of the fuel cell and then subtracting off the various loss terms:

$$E_{real} = E_{Nernst} - \eta_{act} - IR - \eta_{conc} \quad (2\text{-}8)$$

These three categories of irreversibility are considered one by one in the following sections.

2.2.2.1 Activation Losses

At low current density, the voltage of a fuel cell drops rapidly because of the sluggishness of the electrochemical half reactions occurring at the anode and the cathode electrodes. The oxygen reduction reaction at the cathode is especially sluggish and can account for most of the activation losses. Although the final state of product water is lower in energy than that in the initial reactants, an energy barrier impedes the conversion of reactants into products. A portion of the fuel cell voltage is sacrificed to lower this barrier and thus increases the rate at which reactants are converted into products, allowing the fuel cell to output more current. The relationship between the applied activation overvoltage and the current density output is exponential in nature, and can be described by the Butler-Volmer equation:

$$i = i_0 \left(\frac{C_O}{C_O^*} e^{-\frac{\alpha F \eta_{act}}{RT}} - \frac{C_R}{C_R^*} e^{-\frac{(1-\alpha) F \eta_{act}}{RT}} \right) \quad (2\text{-}9)$$

When the overvoltage is greater than $50mV$, the Butler-Volmer equation can be approximated by a much simpler form, called the Tafel equation:

$$\eta_{act} = \frac{RT}{\alpha F} ln \frac{i}{i_0} \quad (2\text{-}10)$$

Activation losses are minimized by maximizing the exchange current density. The exchange current density is a function of the catalyst material and the total reaction surface area. As mentioned earlier, the electrodes are highly porous to maximize the total reaction surface area. Highly dispersing, nano-scale particles of platinum are mixed into the porous electrode so that they are in intimate contact with the gas phase pores, the electrically conductive electrode, and the ion conductive electrolyte. This maximizes the amount of triple phase boundary, thus maximizing the exchange current density. Platinum is currently the best known catalyst for PEMFC.

2.2.2.2 Ohmic Losses

Ohmic losses arise due to the internal resistance of the materials in the fuel cell to the flow of electrons and protons. These losses are called "Ohmic losses" because they generally follow Ohms law, $V=IR$. Both the electrically conductive electrodes and the ion conductive electrolyte contribute to the resistance losses. Usually, ionic resistance is dominant in a well-designed fuel cell. The linear drop in the middle of the *I-V* curve in Fig. 2.3 distinctly manifests the Ohmic loss effects. In fuel cell systems, most of the Ohmic loss arises from the electrolyte.

2.2.2.3 Concentration Losses

At high current density, the voltage output of fuel cell once again drops rapidly and declines quickly to zero. The current density output at zero voltage is known as the short-circuit current, which represents the maximum current that can be produced by the fuel cell. However, at this current level, the voltage output of fuel cell is zero, so the total power delivered by the fuel cell is also zero. Therefore, power peak occurs somewhere in the middle of the *I-V* curve. The reason for the final steep decline in fuel cell voltage at high current density is due to mass transport limitations. At high current density, the fuel or the oxidant gases are consumed on the reaction surfaces faster than they can be replenished. At a certain limiting current density, the partial pressures of the reactant gases at the reaction surfaces plummet towards zero. From the Nernst equation, it is clear that this dramatic decline in the partial pressures of reactants causes a dramatic decline in output voltage. The voltage drop from this mass transportation limit is:

$$\eta_{conc} = A \ln\left(1 - \frac{i}{i_L}\right) \tag{2-11}$$

where A is a fitting parameter (*V*) and it is obvious that the concentration loss is dominant at high current density. Well-designed flow structures and thin, highly porous electrodes may reduce the concentration overvoltage.

2.3 Type of Fuel Cells

There are five major types of fuel cells as follows.

1. Solid Oxide Fuel Cell (SOFC)
2. Molten Carbonate Fuel Cell (MCFC)
3. Phosphoric Acid Fuel Cell (PAFC)
4. Alkaline Fuel Cell (AFC)
5. Proton Exchange Membrane Fuel Cell (PEMFC)

While all five fuel cell types are based upon the same underlying electrochemical principles, they all operate at different temperature regimes, incorporate different materials, and often differ in terms of their fuel tolerance and performance characteristics. These are shown in Table 2.1.

Table 2.1 The Five Major Types of Fuel Cells

Type of fuel cell	PAFC	MCFC	SOFC	PEMFC	AFC
Electrolyte	H_3PO_4	$(Li,K)_2CO_3$	$(Zr,Y)O_2$	MEA	Polymer
Anode	Pt/C	Ni+10wt%Cr	Ni+$(Zr,Y)O_2$	Pt/C,Pt-Ru/C	Pt/C
Cathode	C	NiO	$(La,Sr)MnO_3$,$LaCoO_3$	Pt/C	Pt/C
Ion	H^+	CO_3^{2-}	O^{2-}	H^+	OH^-
Reaction of anode	$H_2 \rightarrow 2H_2O + 2e^-$	$H_2+CO_3^{2-} \rightarrow H_2O+CO_2+2e^-$	$H_2+O^{2-} \rightarrow H_2O+2e^-$ $CO+O^{2-} \rightarrow CO_2+2e^-$	$H_2 \rightarrow 2H_2O+2e^-$	$H_2 + 2OH^- \rightarrow 2H_2O+ 2e^-$
Reaction of cathode	$1/2O_2+2H^++2e^- \rightarrow H_2O$	$1/2O_2+CO_2+2e^- \rightarrow CO_3^{2-}$	$1/2O_2+2e^- \rightarrow O^{2-}$	$1/2O_2+2H^++2e^- \rightarrow H_2O$	$1/2O_2+2H_2O+2e^- \rightarrow 2OH^-$
Operating temperature	160~190°C	600~700 °C	900~1,000 °C	30~80 °C	90~100 °C
Fuel compatibility	H_2	H_2, CH_4	H_2, CH_4, CO	H_2, methanol	H_2
Advantage	CO durability, combined heat and power	high power, combined heat and power, reform the fuel in cell	high power, combined heat and power, air as oxidant, reform the fuel in cell	high density power, air as oxidant, operating in room temperature, fast activation,	Operating in room temperature, fast activation
Disadvantage	operating in high temperature, high cost, low efficiency	device can be corroded	operating in high temperature, damaging in high temperature	high cost, infecting by CO	high cost, fuel is only H_2
Application	distributed generation	large-scale power plant, distributed generation	large-scale power plant, distributed generation, automobile industry	domestic appliances, portable source, automobile	spaceship

Source: Fuel Cell Systems Explained (2003) James Larminie, Andrew Dicks

2.3.1 SOFC

Solid oxide fuel cell (SOFC) is a complete solid-state device that uses an oxide ion-conducting ceramic material as the electrolyte, and includes a lanthanum manganate cathode and a nickel zirconia anode. SOFC works in the region of 800 to 1100℃. This means that high reaction rates can be achieved without expensive catalysts, and that gases such as natural gas can be used directly, or "internally reformed" within the fuel cell, without the need for a separate unit. This type of fuel cell addresses all the problems and takes full advantage of the inherent simplicity of the fuel cell concept. Therefore, it is a promising option for high-powered applications, such as industrial uses or central electricity generating stations.

2.3.2 MCFC

The electrolyte of the molten carbonate fuel cell is a binary molten mixture of lithium and potassium, or lithium and sodium carbonates. It has the potential to be fueled with coal-derived fuel gases or natural gas. Unlike the other fuel cells, carbon dioxide must be supplied to the cathode, and thus converted to carbonate ions. The high temperature achieves a good reaction rate by using a comparatively inexpensive catalyst-nickel. Therefore, MCFC is also a high-temperature fuel cell like SOFC.

2.3.3 PAFC

The phosphoric acid fuel cell (PAFC) uses a phosphoric acid as an electrolyte to conduct proton which is like Nafion membrane in the PEMFC. In PAFC, the electrochemical reactions take place on highly dispersed electrocatalyst particles supported on carbon black. Phosphoric acid is the inorganic acid that has high thermal, chemical, and electrochemical stability. It also contains high volatility (above 150℃) to be adopted as an electrolyte for fuel cells. Due to its low freezing point (42℃) of the pure phosphoric acid, PAFC is usually maintained above such temperature. Unlike PEMFC, the operating temperature of PAFC is normally around 180 to 200℃ that has greater tolerance of CO (up to 1%). PAFC is the first one to be produced in commercial quantities and enjoys widespread terrestrial use.

2.3.4 AFC

The electrolyte of the alkaline fuel cell is an alkaline solution, such as potassium hydroxide, and is operated at about 200℃. AFC is used by NASA on spacecraft, and it is now finding new applications in hydrogen-powered vehicles.

2.3.5 PEMFC

The proton exchange membrane fuel cell capitalizes on the essential simplicity of the fuel cell. The electrolyte is an ion conduction polymer to move H^+ ion pass through the supporting ionomer structure. PEMFC appears to be more adaptable to automobile use than PAFC. PEMFC

works at low temperature which can start quickly. The thinness of the MEA makes the compact design without corrosive fluid in the fuel cell. These cells are the best candidates for light-duty vehicles, buildings, and much smaller applications. A very attractive solution to the hydrogen supply problem is to use methanol as a fuel instead. Such cell is called direct methanol fuel cell (DMFC). It also uses a polymer membrane as an electrolyte.

The thesis is interested in state-of-the-art PEMFC science and technology, because it is simple structure, runs at relatively low temperature, widely practicability and high efficiency.

2.4 Principle of PEMFC

The principle of fuel cell is a device that transforms chemical energy into electricity; it is the same as the conventional battery, both belong to the electrochemical source. It is different from the conventional battery in the part of electrodes, which are belonging to non-activity material, so it is only an element of catalysis. As the active material, stored in fuel cell, is used up, the device must be stop using, and resupplied with the chemical material to work; in other word, the fuel cell is just a transformation machine.

Basically the reaction of fuel cells can be regarded as an inverse reaction of electrolyzing the water; hydrogen is transformed into hydrogen ion and electrons by the catalyst, Pt. Then the electrons pass through the outer circuit to generate electric power, besides hydrogen ion through the MEA reacts with oxygen, and generates the water at the

cathode. The equations of electrochemical reaction are as follows:

$$\text{Anode:} \quad H_2 \Leftrightarrow 2H^+ + 2e^- \tag{2.1}$$

$$\text{Cathode:} \quad \tfrac{1}{2}O_2 + 2H^+ + 2e^- \Leftrightarrow H_2O \tag{2.2}$$

$$\text{Overall:} \quad H_2 + \frac{1}{2}O_2 \Leftrightarrow H_2O \tag{2.3}$$

2.5 Structure of PEMFC

A PEMFC, shown in Fig. 2.4, is simply like a sandwich structure. Each component is described as follows:

2.5.1 Bipolar Plate

In a single fuel cell stack, several fuel cells are assembled in series. The bipolar plate is the electronically conductive plate positioned next to the anode end of one cell and the cathode end of another cell. In general, each surface of the bipolar plate contains grooved channels with inlet and outlet as flow path of the fuel and oxidant, respectively.

2.5.2 Gas Diffusion Layer (GDL)

The gas diffusion layer (GDL) is usually made of carbon paper or cloth with a porous structure treated with hydrophobic agent. It has to meet several requirements, such as electronic conductivity, heat conductivity, fluid permeability, wettability, and mechanical stability.

2.5.3 Gasket

The gasket is made of teflon-PTFE, whose characteristics are able to endure the high temperature, corrosion, and etc. It also can avoid the gas spreading out from the gas diffusion layer (GDL) because GDL has a thickness. So the gasket plays an important role in sealing.

2.5.4 Proton Exchange Membrane (PEM)

The “core” of a fuel cell comprises a solid perfluorsulphonic acid polymer, usually named as Nafion from *DuPont.* It functions as a path for protons. The protons are transferred by migration and convection with water. The membrane, therefore, not only needs to be maintained hydrous but also is free from flooding.

2.5.5 Active Layer

The active layer contains the porous catalyzing material and is positioned between PEM and GDL. For a PEMFC, active layer is usually the platinum (Pt) metal in the anode and cathode. The function of Pt metal is to activate the electrochemical reactions.

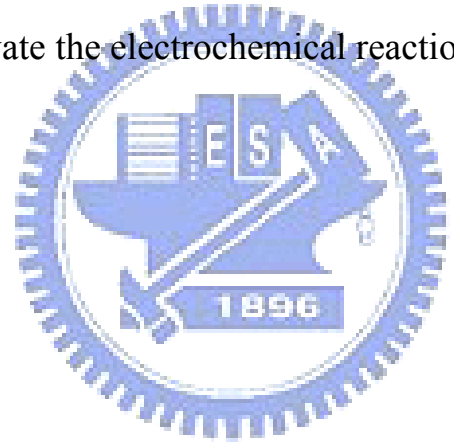

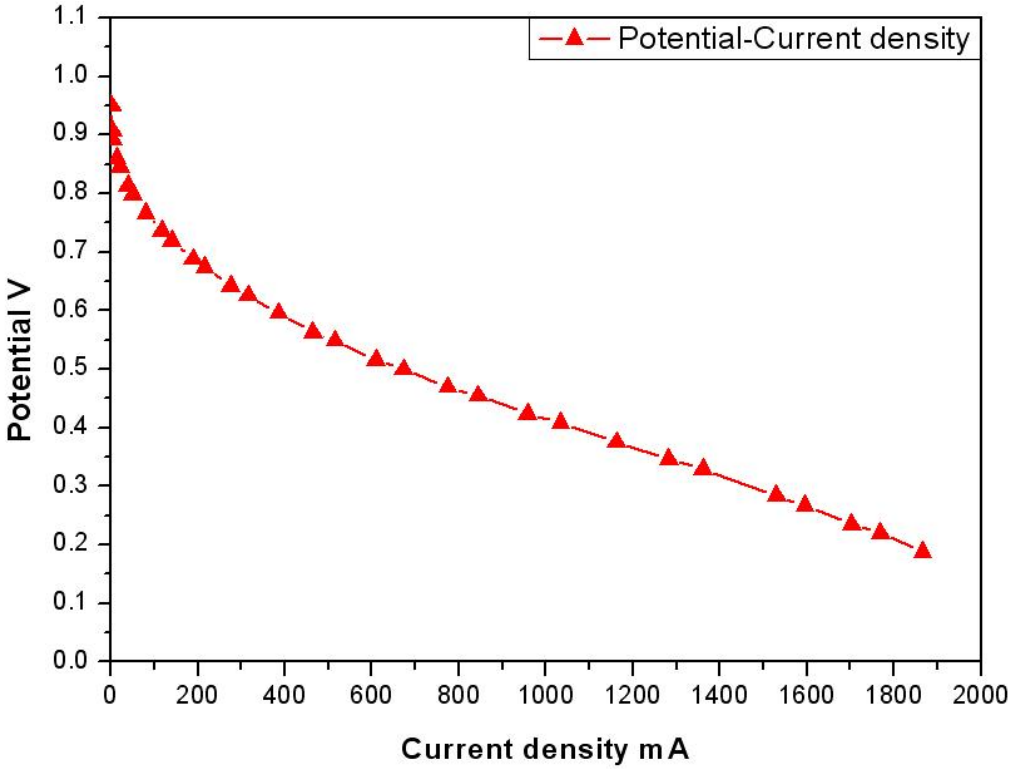

Fig. 2.1 a Typical I-V Curve For a PEMFC

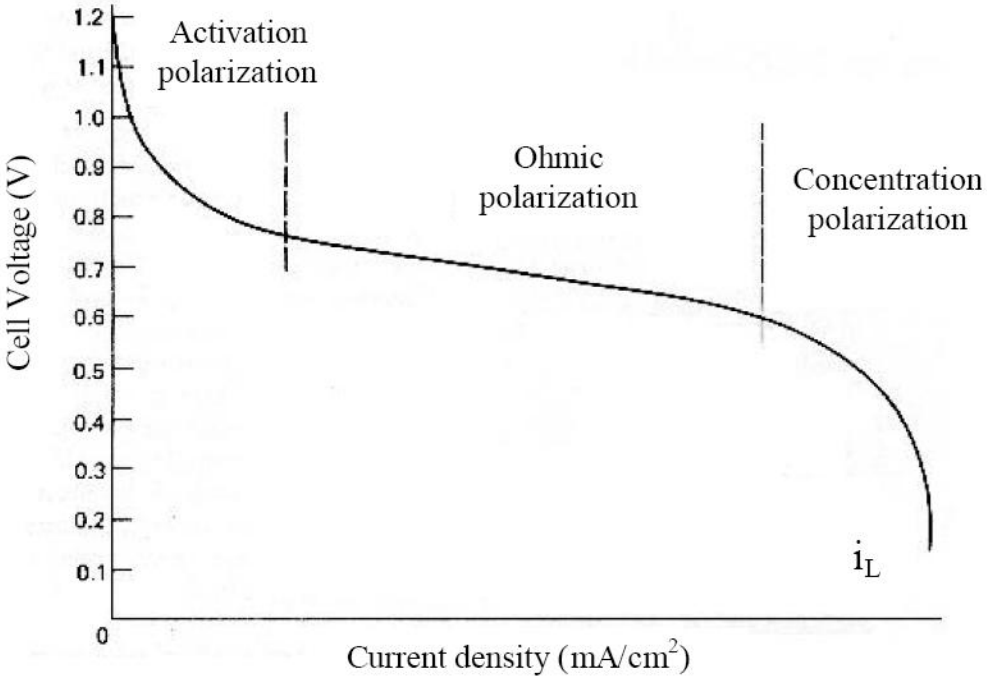

Fig. 2.2 I-V Curve of Fuel Cell

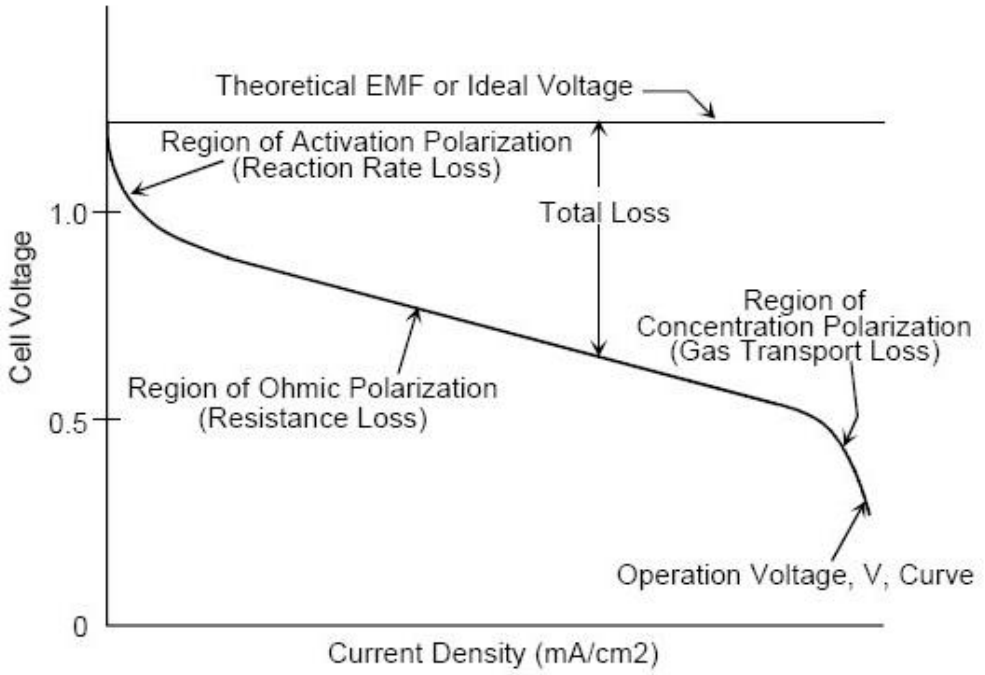

Fig. 2.3 The Linear Drop in the Middle of the I-V Curve

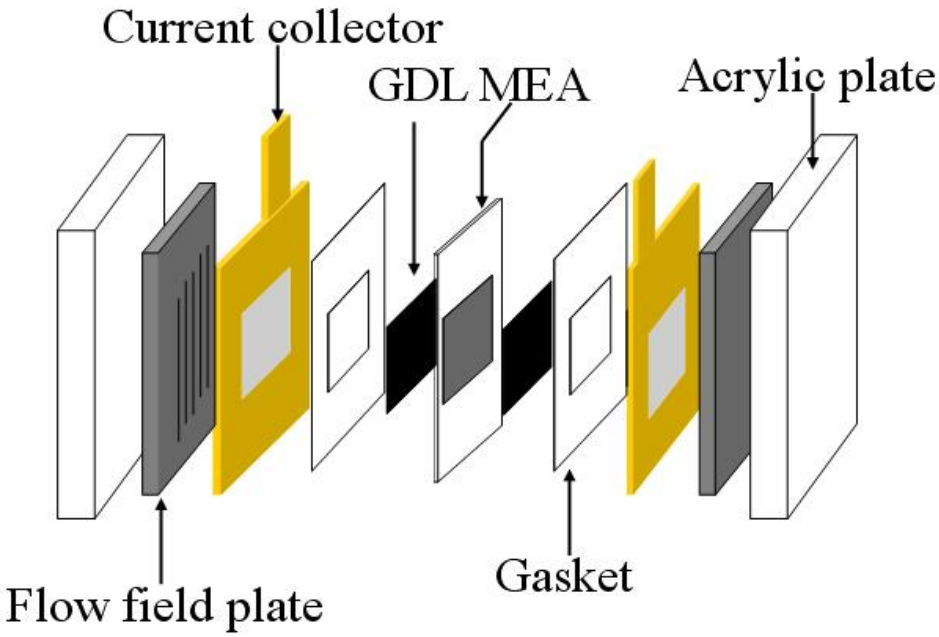

Fig. 2.4 Sandwich Structure of PEMFC

Chapter 3

Experimental Apparatus and MEMS Fabrication Processes

3.1 Processes of Fabricating the Flow Field Plates

The fabrication of micro PEMFC is different from the one for the conventional fuel cells in the aspect of scale, especially in the flow field plate. In the past, the flow field of conventional fuel cells was manufactured by the machine tool, such as CNC, but now, the micro PEMFC adopts the MEMS fabrication. Figure 3.1 shows the steps of fabrication process of flow field plate for a micro PEMFC:

3.1.1 Mask Design

The mask is designed by the AutoCAD for the different open ratios of 50%, 67% and 75% at the same area, 3cm^2, respectively; see Fig. 3.2. In other words, this work also can change the other patterns of flow field and find the corresponding performance.

3.1.2 RCA Clean

The **RCA (Radio Corporation of America) clean**, as shown in Table 3.1, in the wet bench (Fig. 3.3) is a standard set of wafer cleaning steps which needs to be performed before the high-temp processing steps (oxidation, diffusion, CVD) of silicon wafers in semiconductor manufacturing. Werner Kern developed the basic procedure in 1965 while working for RCA, the Radio Corporation of America. It involves the following steps:

I. **Removal of the organic contaminants (Caro Clean)**

II. **Removal of thin oxide layer (Oxide Strip)**

III. **Removal of the organic contaminants (Organic Clean)**

IV. **Removal of ionic contamination (Ionic Clean)**

V. **Spin drying, see Fig. 3.4.**

Table 3.1 the Steps of RCA Clean Process

Steps	***Title***	***Chemical solution***	***Experimental parameter***	***Function***
1	Caro System	H_2SO_4：H_2O_2=3：1	Temperature:120℃ Drenching:600sec	Removal of insoluble organic contaminants
2	Clean	D.I. water	Temperature: room temperature Time:60sec	Clean
3	DHF (Diluted HF)	HF：H2O = 1：50	Room temperature	Removal of thin oxide layer
4	Clean	D.I. water	Temperature: room temperature Time:60sec	clean
5	SC 1 System	NH_4OH：H_2O_2： H_2O=1：1：5	Temperature:75℃ Drenching:600sec	Removal of the organic contaminants
6	Clean	D.I. water	Temperature: room temperature Time:60sec	Clean
7	SC 2 System	HCL：H_2O_2： H_2O=1：1：6	Temperature:75℃ Drenching:600sec	Removal of ionic contamination
8	Clean	D.I. water	Temperature: room temperature Time:60sec	Clean
9	Spin drying		Step1：1200rpm;time:120sec Step2：1800rpm;time:150sec	Spin drying

3.1.3 Deposition the Block Layer Si_3N_4

In this step, a layer is created that is applied as the block function. The function is to block the etching solution, KOH, for later step, but the block layer must be a material of high etching select ratio between the block layer and Si. So we select the nitride (**Si_3N_4**) as the block layer, which is developed by the PECVD as shown in Fig. 3.5. Followings are the parameters of developing the nitride (**Si_3N_4**):

- **Nitride**

  Process: Standard Nitride

  Wafer size: 6" wafer

  Process gas: NH_3, N_2, SiH_4

  Plasma power: 50~150W

  Temperature: up 250℃, base 300℃

  Process pressure: 3~5torr

  Thickness: 5000 Å

3.1.4 Fabrication of Photolithography

The step is important in the all of fabrication processes. It is fabricated by Track MK-8 (Fig. 3.6), whose functions include coating PR (photo resist), exposure, development processes. This is a serial process which can lower the experimental uncertainty in the pattern work. Table 3.2 shows the parameters of Track MK-8.

Table 3.2 Parameter of Track MK-8

Wafer flow No	***Function***	***Step 1***	***Step2***	***Step3***	***Step 4***	***Step5***	***Step6***
1	NEB Resist Coatiog	Unit Cassette 1-1,1-2,1-3, 1-4	AD(2-3) 90℃	COL(2-6) 23℃	COAT(2-1) 4400rpm	HP(2-8) 110℃，120sec	Unit Cassette 1-1,1-2,1-3, 1-4
2	DSE Resist Coating	Unit Cassette 1-1,1-2,1-3, 1-4	AD(2-3) 90℃	COL(2-6) 23℃	COAT(2-1) 2000rpm	HP(2-8) 95℃，120sec	Unit Cassette 1-1,1-2,1-3, 1-4
8	G-line Resist Coating	Unit Cassette 1-1,1-2,1-3, 1-4	AD(2-3) 90℃	COL(2-6) 23℃	COAT(2-1) 5000rpm	HP(2-8) 90℃，60sec	Unit Cassette 1-1,1-2,1-3, 1-4
20	I-line Resist Coatiog	Unit Cassette 1-1,1-2,1-3, 1-4	AD(2-3) 90℃	COL(2-6) 23℃	COAT(2-1) 3435rpm	HP(2-8) 90℃，90sec	Unit Cassette 1-1,1-2,1-3, 1-4
5	NEB Resist Develop	Unit Cassette 1-1,1-2,1-3, 1-4	HP(2-4) 105℃，120sec	COL(2-9) 23℃	DEV(2-2) 60sec	DHP(2-7) 110℃，120sec	Unit Cassette 1-1,1-2,1-3, 1-4
4	DSE Resist Develop	Unit Cassette 1-1,1-2,1-3, 1-4	HP(2-4) 115℃，120sec	COL(2-9) 23℃	DEV(2-2) 60sec	DHP(2-7) 115℃，60sec	Unit Cassette 1-1,1-2,1-3, 1-4
11	G-line Resist Develop	Unit Cassette 1-1,1-2,1-3, 1-4	HP(2-5) 120℃，60sec	COL(2-9) 23℃	DEV(2-2) 60sec	DHP(2-7) 120℃，90sec	Unit Cassette 1-1,1-2,1-3, 1-4
21	I-line Resist Develop	Unit Cassette 1-1,1-2,1-3, 1-4	HP(2-4) 110℃，60sec	COL(2-9) 23℃	DEV(2-2) 60sec	DHP(2-7) 120℃，90sec	Unit Cassette 1-1,1-2,1-3, 1-4

3.1.5 Removing the Block Layer

The wafers are mounted on the RF-powered electrode directly, and under the influence of a RF field, the highly energized ions impinge on the surface to stimulate reaction in a direction perpendicular to the wafer surface. Therefore, the vertical sidewalls, being parallel to the direction of ion bombardment, are little affected by the plasma. This approach is called reactive ion etching (R.I.E). This work uses the R.I.E to bombard the block layer, which is not needed. Finally, the desired patterns, which this work wants to etch, are obtained.

3.1.6 Etching the Si by KOH

A commonly used orientation-dependent etch for silicon consists of a mixture of potassium hydroxide (KOH) in water. The concentration of KOH solution is 30% and its temperature is 80^0C. The etch-rate is about 2.1μm/min for the (110) plane, 1.4μm/min for the (100) plane, and only 0.003μm/min for the (111) plane at 80^0C [18-19]. Therefore, the ratio of the etch rates for the (100) and (110) planes to the (111) plane are very high that are 400:1 and 600:1, respectively.

3.1.7 Removing the Block Layer (Si_3N_4)

Finally, this work removes the block layer ($\mathbf{Si_3N_4}$) by using phosphoric acid solution (85%, 160^0C), whose etching rate is 42Å/min [16-17]. Figure 3.7 shows the completed patterns of the basic flow field plates.

3.2 Assembly and Components of micro PEMFC

3.2.1 Components of Micro PEMFC

- **Membrane Electrode Assembly (MEA)**
- **Gas Diffusion Layer (GDL)**
- **Gasket**
- **Current collector slices**
- **Flow field plate**
- **Acrylic plate**

In these components, some of them have to be done extra works. For examples, the flow field plates need to be drilled gas inlet and outlet before assembly, and the acrylic plate in air-breathing cell needs an extra hole for natural convection. These components are shown in Figs. 3.8, 3.9, 3.10, and 3.11, respectively.

3.2.2 Assembly of Micro PEMFC

The single micro PEMFC is assembled by bipolar plates, acrylic plates, current collector slices and membrane-electrode-assembly (MEA). The shape of the structure is like sandwich, as shown in Figs. 3.12 and 3.13. Because such micro PEMFC uses forced convection to transport oxidant (air or pure oxygen) and hydrogen, the sealing problem must be treated carefully.

3.2.3 Three Type Current Collector Slices

The performance comparison of current collector slice materials and their conductive areas are investigated in this work. The micro PEMFC performance is greatly affected by current collector slices. Three types of current collector slices, which are two-narrow-strips, Cu (square) and

Cu/Au (square), respectively, are tested and they are shown in Fig. 3.14.

3.2.4 Assembly of Air-Breathing Micro PEMFC

The air is used as oxidant supply. Although its performance is expected to be lower than that of pure oxygen, the air is easy to get from atmosphere and free. In this work, the performance comparison between air and pure oxygen is still carried out in this work. The difference between the air-breathing micro PEMFC assembly and the original one is that previous one has a hole in cathode acrylic plate to make an extra natural convection. Figure 3.15 shows the air-breathing micro PEMFC assembly.

3.3 Test Station

A PEMFC test station, as shown in Figs. 3.16 and 3.17, is constructed to evaluate the characteristics of single or stack fuel cell. The components of test station are listed in Table 3.3.

Table 3.3 Instrument of Hardware Specifications

Hardware	***Number***	***Specification / Type***
Controlling Temperature System	5	25~90^{0}C T-type thermal couple
Heater	6	Humidify the gas: 250W Heating fuel cell: 50W Preheating pipe: 180W
Controlling Mass Flow Rate System	2	Hydrogen:0-400 sccm Oxygen: 0-2000 sccm
Display of mass flow rate	1	PROTEC PC-540
Valve of Back Pressure	2	250 psi Max
Back Pressure gauge	2	0~150 psi
Adding Humidity Container	2	Volume:1L Pressure:5Kgf/cm^2
Drain Valve	2	AW30-03BD
Switching Power Supply	2	3V,20A 24V,4.5A
Electromagnetic Valve	3	061317X 501062S
Hydrogen Detection	1	COSMOS 0-2000 ppm
19" Instrumental Frame	1	RA3570-0

Some parameters, such as flow rate, humidity and reheat temperature, can be adjusted in this station. After experiments, the testing data, as listed in Table 3.4, can be collected by the software of test station. The limiting conditions of test station are listed in the Table 3.5.

Table 3.4 Function of Software

Item	***Function***
Automatic Control System	Controlling the Current, Voltage, Mass Flow Rate, Load
Testing Data	Current vs. Time, Voltage vs. Time, Power vs. Time, Tafel Data, Long-time Performance test

Table 3.5 One or More PEMFC Testing Range

Type of electronic load	***PRODIGIT 3315D***
Current	0~15A
Voltage	0~60V
Power	75W Max

Fig. 3.18 shows the diagrams of components for the test station. Mainly, the system includes three parts, mass flow controllers, temperature controllers, and a DC electronic load.

3.4 Uncertainty Analysis

Some form of analysis must be performed on all experimental data. The analysis may be a simple verbal appraisal of the results, or it may take the form of a complex theoretical analysis of the errors involved in the experiment and matching of the data with fundamental physical principles. Therefore, their accuracy should be confirmed before the analyses of experimental results. Experimental measuring must have errors, and experimental errors divide into the fixed (systematic) error

and random (non-repeatability) error, respectively. Fixed error is produced after each experiments and it can be removed by proper calibration and correction. However, Random error is different for every apparatus reading datum and hence cannot be removed. The objective of uncertainty analysis is to estimate the probable random error in experimental results.

3.4.1 Analyses of the Propagation of Uncertainty in Calculations

Uncertainty analysis estimates the uncertainty levels in the experiment. A method of estimating uncertainty in experimental results has been presented as follows:

Suppose a set of measurements is made and the uncertainty in each measurement may be expressed with the same odds. These measurements are then used to calculate some desired results of the experiments. The result R is a given function of the independent variables $x_1, x_2, x_3 \ldots x_n$. Thus,

$$R = R(x_1, x_2, x_3, \ldots, x_n) \tag{3-1}$$

An individual x_n, which affects error of R, can be estimated by the deviation of a function. A variation, δX_n, in x_n would cause R to vary according to

$$\delta R_n = \frac{\partial R}{\partial x_n} \delta x_n \tag{3-2}$$

Normalize above equation by dividing R to obtain

$$\delta \frac{R_n}{R} = \frac{1}{R} \frac{\partial R}{\partial x_n} \delta x_n = \frac{x_n}{R} \frac{\partial R}{\partial x_n} \frac{\delta x_n}{x_n} \tag{3-3}$$

Equation (3-3) can be used to estimate the uncertainty interval in the result due to the variation in x_n. Substitute the uncertainty interval for x_n,

$$u_R = \frac{x_n}{R}\frac{\partial R}{\partial x_n}ux_n \quad (3\text{-}4)$$

To estimate the uncertainty in R due to the combined effects of uncertainty intervals in all the x_i, it can be shown that the best representation for the uncertainty interval of the result is

$$u_r = \pm\left[\left(\frac{x_1}{R}\frac{\partial R}{\partial x_1}u_1\right)^2 + \left(\frac{x_2}{R}\frac{\partial R}{\partial x_2}u_2\right)^2 + \cdots + \left(\frac{x_n}{R}\frac{\partial R}{\partial x_n}u_n\right)^2\right]^{\frac{1}{2}} \quad (3\text{-}5)$$

3.4.2 The Uncertainty of Test Station Apparatus

The apparatus must to be corrected by other standard instruments to make sure that they can normally operate and let the inaccuracy of the experimental results reduce to the minimum.

3.4.2.1 The Uncertainty of HP 6060B Electronic Load: u_v,u_A

The HP 6060B electronic load in the test station has been corrected its potential and current meter before experiment. The research uses FLUKE 8060A Digital Multimeter and Chroma Smart N300-040 Electronic Load to correct HP load box. Table 3.6 shows the error for different potentials.

Table 3.6 Uncertainty of Electronic Load Potential Meter

Standard value (V)	*Digital meter (V)*	*Uncertainty (%)*
20.00	19.81	-0.95
9.95	9.85	-1.00
8.02	7.95	-0.87
6.04	5.95	-0.99
5.00	4.97	-0.60
3.03	3.00	-0.99
1.00	0.998	-0.50
0.00	0.00	0.00

Next, the DC current meter of HP load box is corrected. They use

Chroma Smart electronic load and FLUKE digital meter to find the impedance of the shunt. They connect the shunt between HP load box and DC power source after correcting and adjust different potentials of power source, therefore, it can change the measurement current of load box meter. At the same time, the shunt measures a signal of current. After converting this signal, it can define the actual current of this circuit. Table 3.7 shows the error for different current.

Table 3.7 Uncertainty of Electronic Load Current Meter

Fluke digital meter (mV)	***Electronic load (A)***	***Conversion value ($\bar{A}$)***	***Uncertainty (%)***
0.00	0.00	0.00	0.00
1.69	1.00	1.02	1.96
5.05	3.00	3.04	1.32
8.37	5.00	5.03	0.60
16.71	10.00	10.05	0.50
25.04	15.00	15.06	0.40
33.41	20.00	20.09	0.45
50.21	30.00	30.19	0.63

3.4.2.2 The Uncertainty of Mass Flow Controller

In this study, there have three MFCs in the test station including anode, cathode and oxygen bleeding flow meter. The specified error is shown as follows:

$$ERROR(\%) = \frac{CALAUATED - TARGET}{FULLSCALE} \times 100\%$$

The ranges of MFC specified accuracy are 1000±5% with anode MFC, 2000±5% with cathode MFC and 500±1% with air bleeding MFC. They use the same company instrument, series 5850 MFC, as the

standard correction apparatus to correct these MFCs. The results are listed in the Table 3.8, 3.9, and 3.10, respectively.

Table 3.8 Uncertainty of Anode MFC

Standard value (sccm)	***Brooks MFC read value (sccm)***	***Measure value (sccm)***	***Uncertainty (%)***
1000	1002	1001	-0.10
500	501	499.8	-0.23
250	250.2	249.7	-0.23
0	0	0	0

Table 3.9 Uncertainty of Cathode MFC

Standard value (sccm)	***Brooks MFC read value (sccm)***	***Measure value (sccm)***	***Uncertainty (%)***
2000	1999.8	1999.4	-0.02
1250	1255	1253	-0.15
1000	1000.3	1000.2	-0.01
500	500.2	500	-0.03
0	0	0	0

Table 3.10 Uncertainty of Air Bleeding MFC

Output Voltage	***Brooks MFC read value (sccm)***	***Measure value (sccm)***	***Uncertainty (%)***
5	500	500.34	0.07
3.75	375	374.54	-0.09
2.5	250	250.32	0.06
1.25	125	124.54	-0.09
-0.001	0.0	0	0

They are anode, cathode and air bleeding flow meter, respectively. In these tables, the standard value means the setting flow rate, the Brooks MFC read value means the test station MFC readout value, the measurement value is the actual measured value. Then, these data can

define the errors in different flow rates.

3.4.2.3 The Uncertainty of Temperature Controller

There are three temperature controllers in the test station. They are anode, cathode humidifier and fuel cell, respectively. The results of analyses are listed in Table 3.11, 3.12, and 3.13, respectively. In these tables, standard value means the setting temperature and the measure value means actual value, measured by the correction apparatus.

Table 3.11 Uncertainty of Anode Temperature Controller

Standard value (℃)	***Measure value (℃)***	***Uncertainty (%)***
25	25	0
35	35	0
50	50	0
70	70	0
85	84	-1.17
95	94	-1.05
100	99	-1

Table 3.12 Uncertainty of Cathode Temperature Controller

Standard value (℃)	***Measure value (℃)***	***Uncertainty (%)***
25	25	0
35	35	0
50	50	0
70	70	0
85	85	0
95	94	-1.05
100	99	-1

Table 3.13 Uncertainty of Cell Temperature Controller

Standard value (℃)	*Measure value (℃)*	*Uncertainty (%)*
25	25	0
35	35	0
50	50	0
70	70	0
85	85	0
95	95	0
100	100	0

3.4.3 The Uncertainty of Fuel Cell Power Density

The uncertainty of fuel cell power density comes from measuring process of fuel cell apparatus, therefore, the minimum scale of measuring voltage in the apparatus is $1mV$, and the minimum scale of measuring current in the apparatus is $0.1mA$. Appendix A shows the measuring uncertainty calculating process. Table 3.14 shows the uncertainty power density of PEMFC and micro PEMFC.

Table 3.14 The Measuring Uncertainty of Fuel Cell

PEMFC	The measuring uncertainty	Voltage	±0.10%
		Current	±0.02%
		Power	±0.10%
Micro PEMFC	The measuring uncertainty	Voltage	±0.10%
		Current	±0.01%
		Power	±0.10%

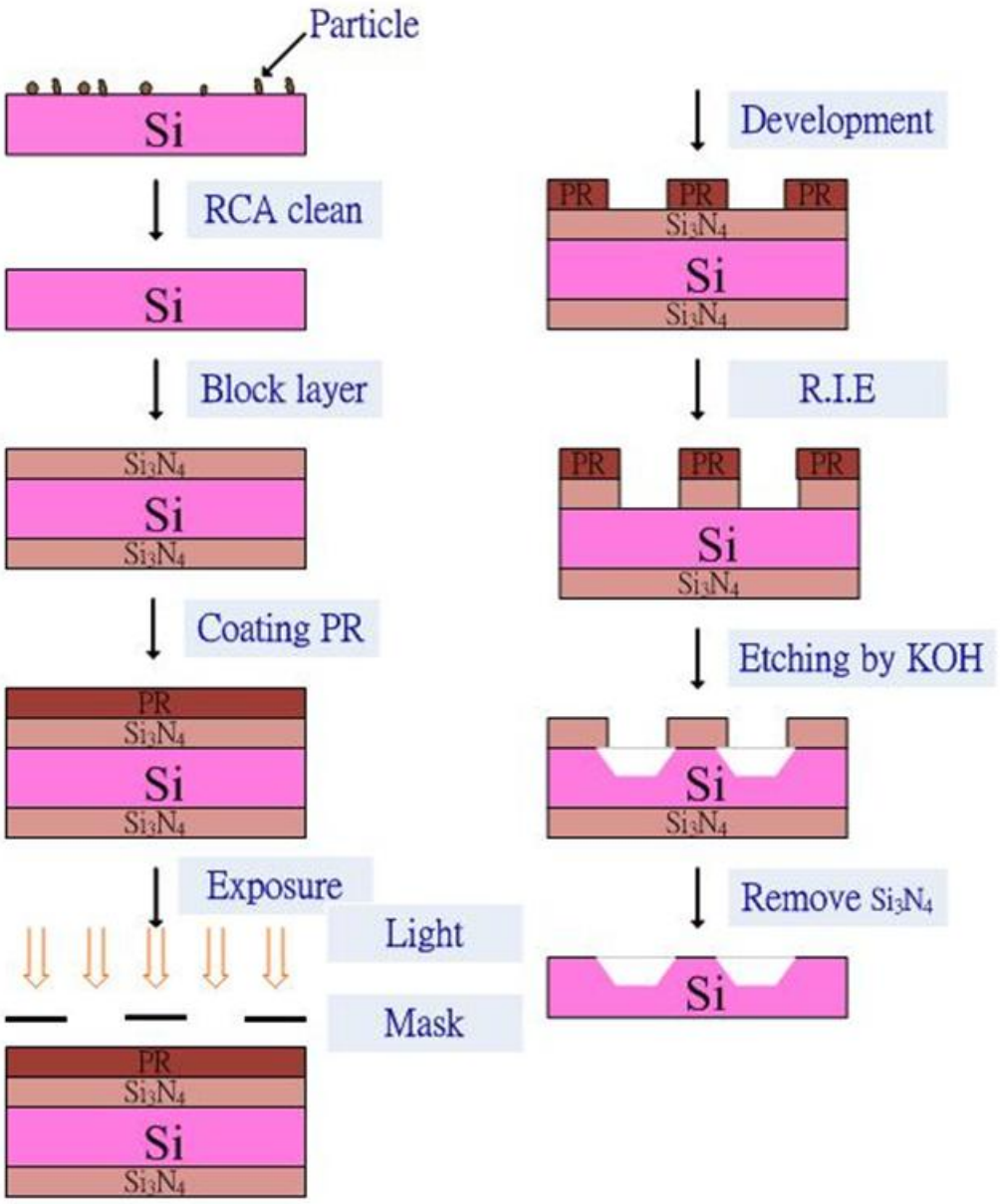

Fig 3.1 The Flow Charts of Flow Field Plate Fabrication

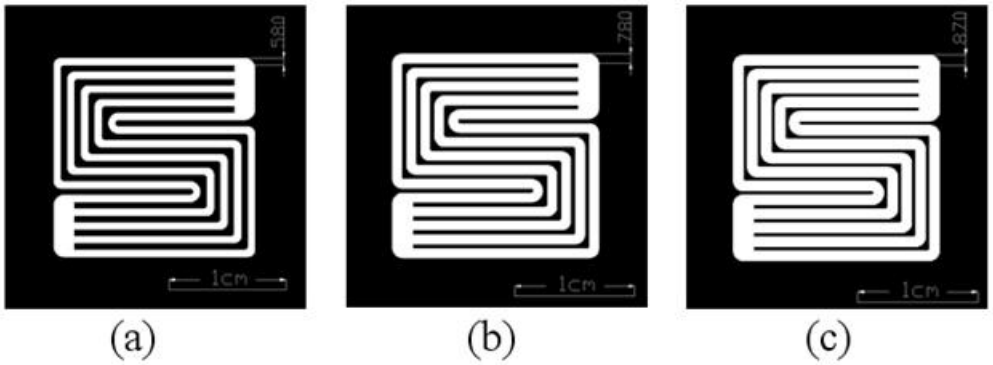

Fig. 3.2 Open Ratio (a) 50% (b) 67% (c) 75%

Fig. 3.3 Wet Bench

Fig. 3.4 Spin Drying

Fig. 3.5 PECVD & ICP

Fig. 3.6 Track MK-8

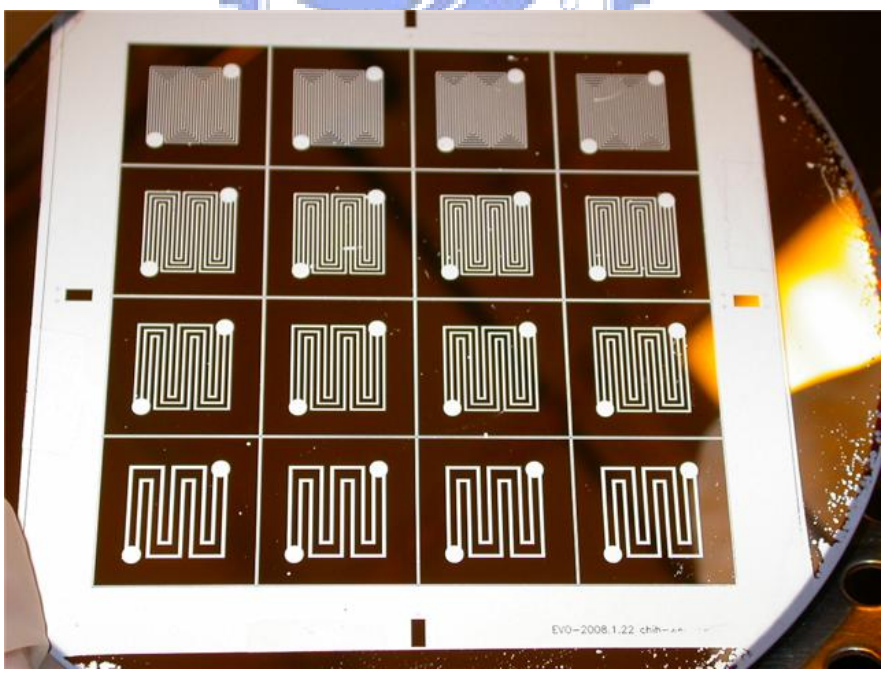

Fig. 3.7 Patterns of Flow Field Plates

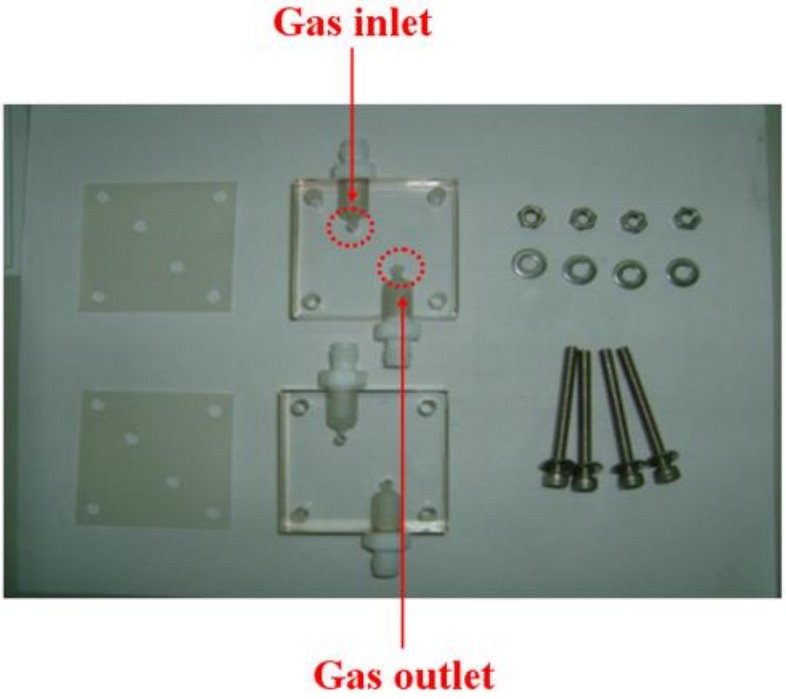

Fig. 3.8 Acrylic Plate

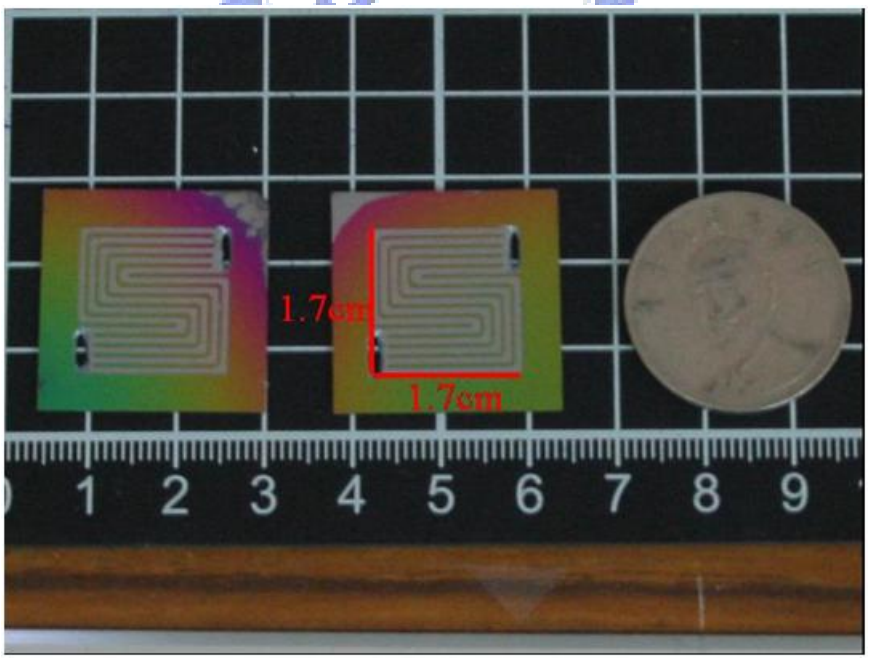

Fig. 3.9 Flow Field Plates

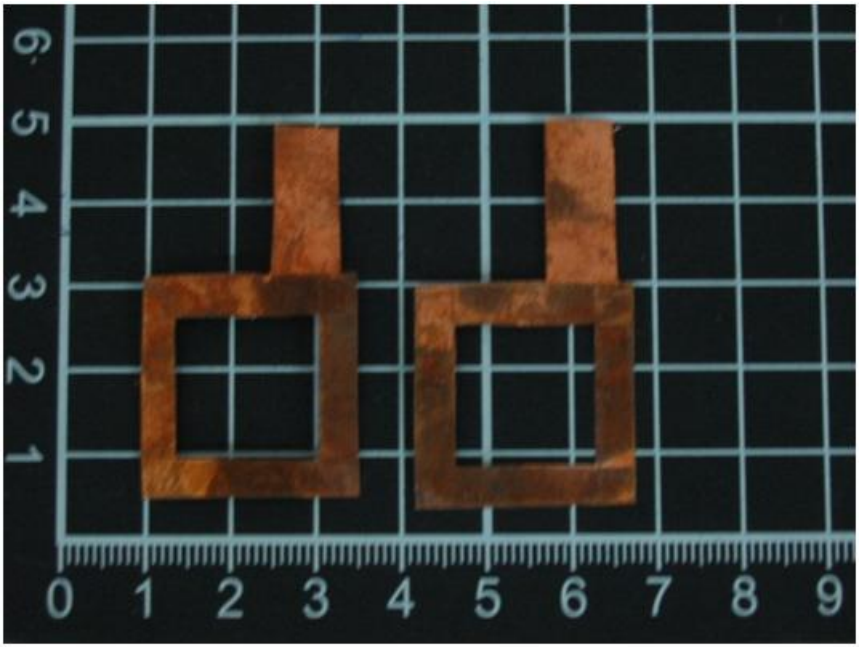

Fig. 3.10 Current Collector Slices

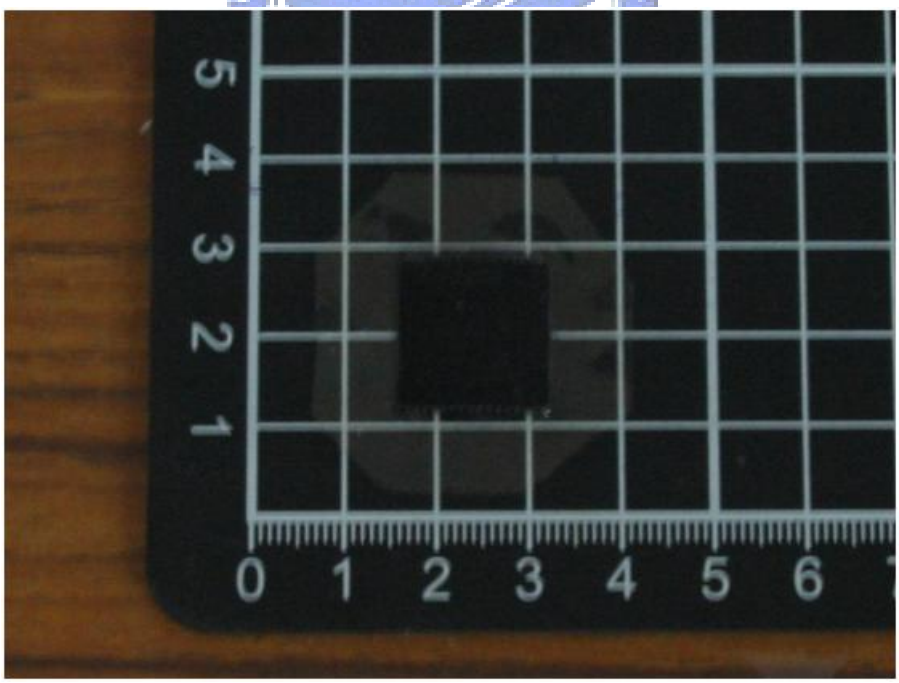

Fig. 3.11 GDL and MEA

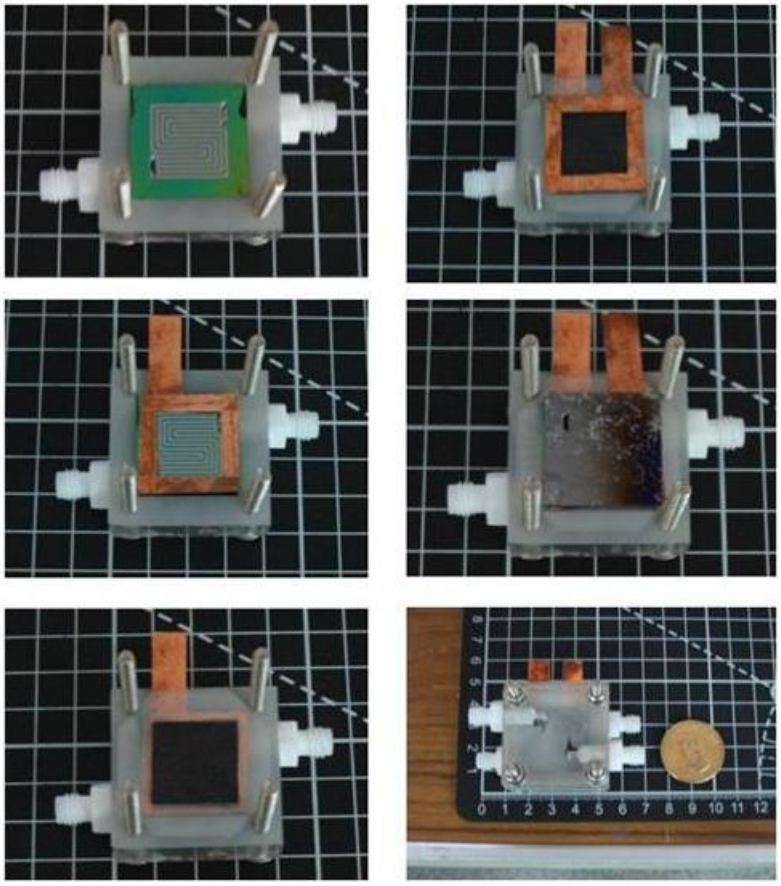

Fig. 3.12 The Steps of Assembly Micro PEMFC

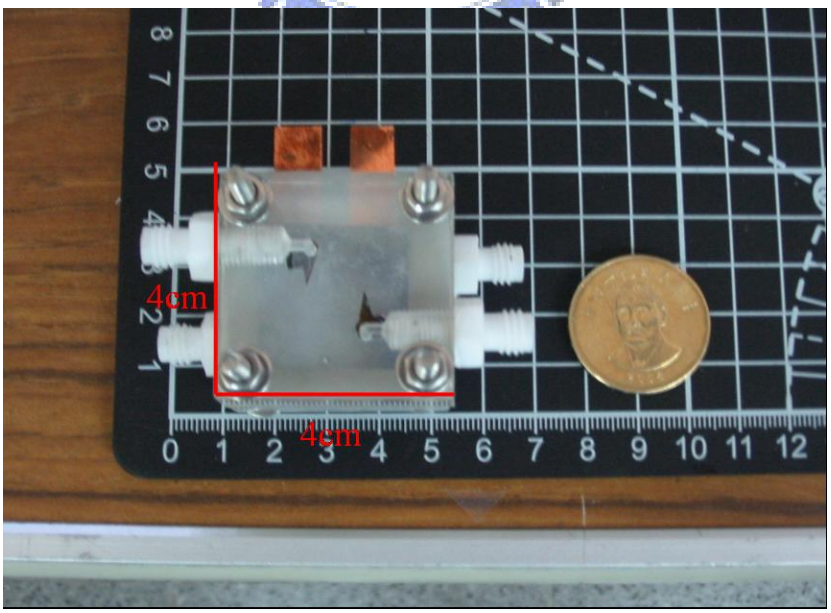

Fig. 3.13 The Assembly of Micro PEMFC

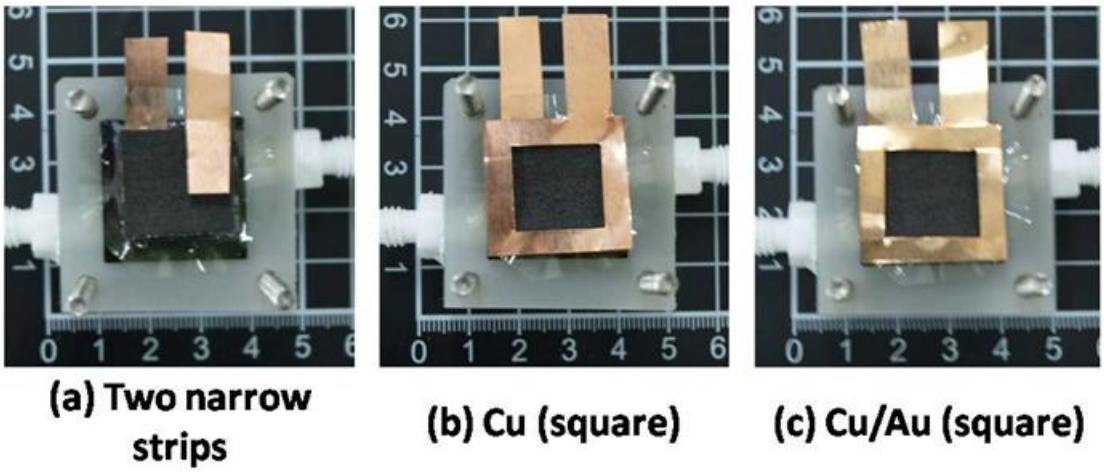

Fig. 3.14 Three Type Current Collector Slices

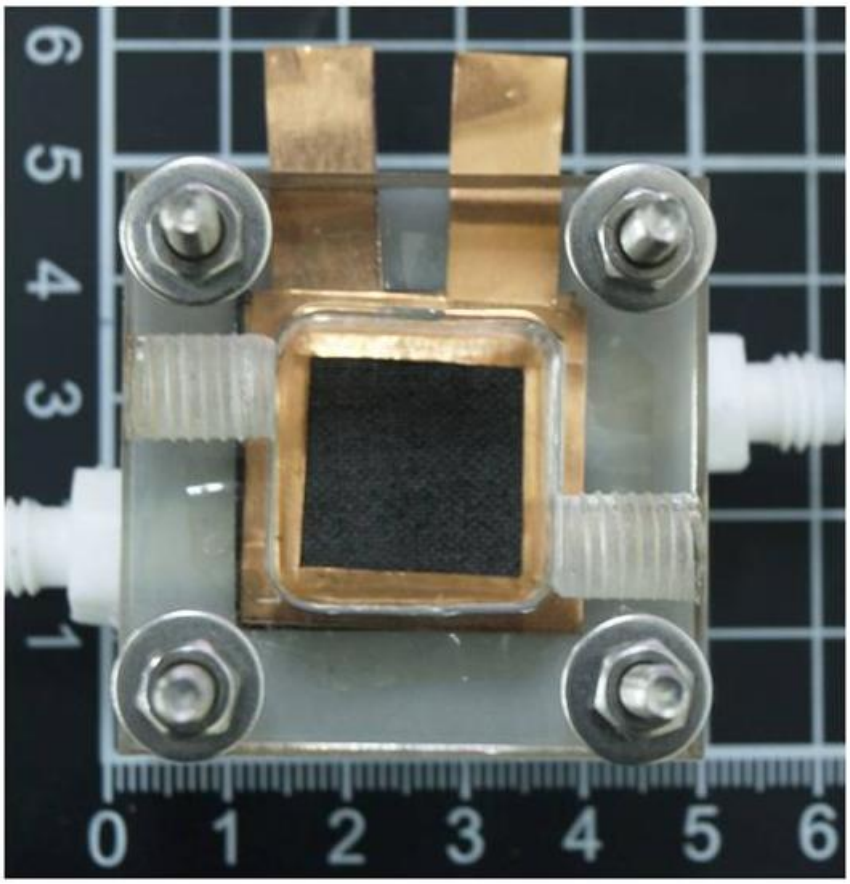

Fig. 3.15 Assembly of Air-Breathing Micro PEMFC

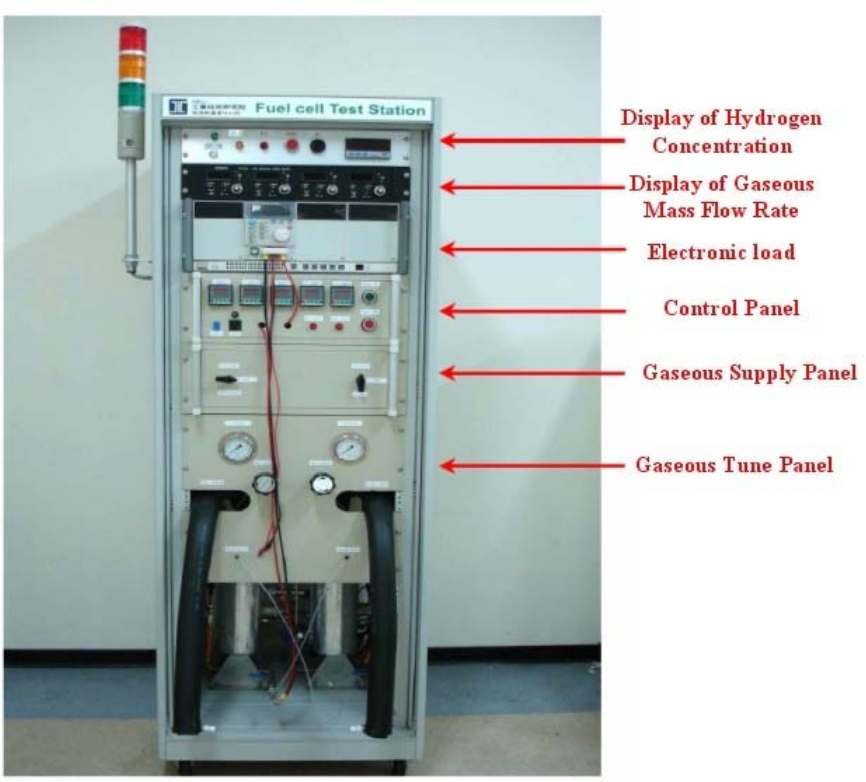

Fig. 3.16 Test Station

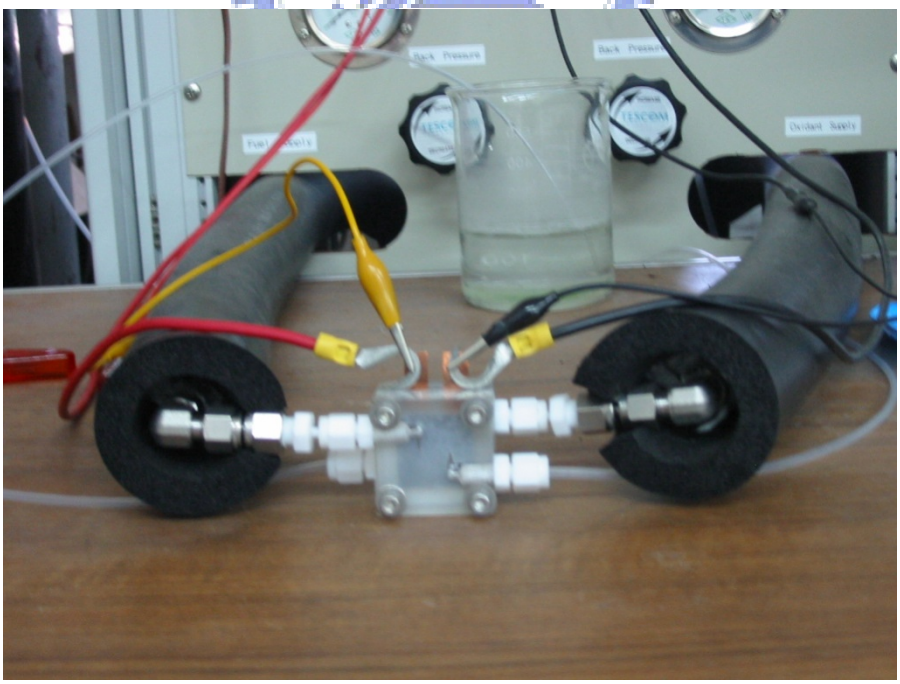

Fig. 3.17 Test of a Single micro PEMFC

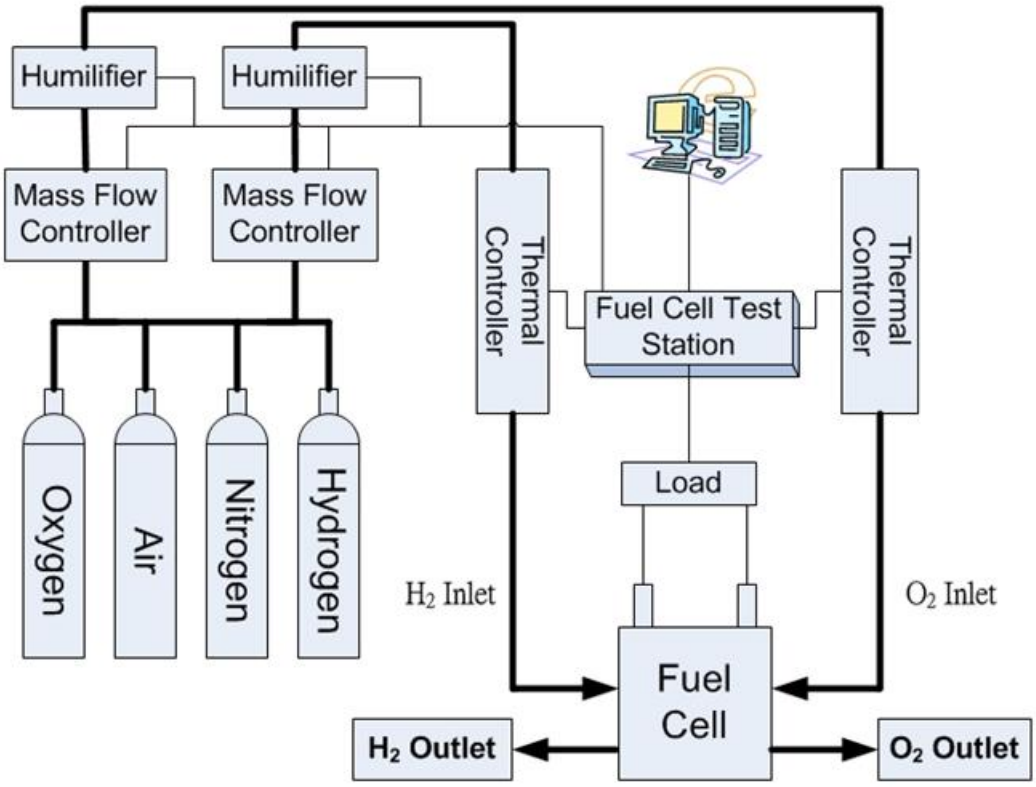

Fig. 3.18 Components of Test Station

Chapter 4

Results and Discussions

The study is divided into two categories; one is the parametric experimental investigation, and the other is the durability test. In the parametric experimental works, the parameters include material of current collector slices, reheat temperature, open ratio and different cathode gases, respectively.

The MEA used is manufactured by the Asia Pacific Fuel Cell Technologies. The activation time of MEA takes one day in this study; its purpose is to activate the catalyst layer. Its specifications are listed in Table 4.1.

Table 4.1 The Properties of MEA

MEAs DupPont™ Nafion® NRE-212	
Anode Loading (Pt)	0.5 (mg/cm^2)
Cathode Loading (Pt)	0.5 (mg/cm^2)
Active area	$4cm^2$ (2cm × 2cm)

4.1 Reference Case

Since a series of parametric studies is carried out, a reference case, served as the comparison base, is chosen in advance. Table 4.2 lists the testing conditions for the reference case of the single micro PEMFC.

Table 4.2 Testing Conditions of Reference case

Reactant gases	
Anode	H_2 (99.9%)
Cathode	O_2
Flow rates	
Anode	H_2:30sccm
Cathode	O_2: 30sccm
Gas backpressure (gauge)	
Anode	0 kPa
Cathode	0 kPa
Current Collector Slices	
Material	Cu/Au (square)
Temperatures	
Gas reheat temperature	25℃
Gas humidified temperature	25℃
Open Ratio of bipolar plates	
Anode Open Ratio	67%
Cathode Open Ratio	67%

The resultant performance curve of the reference case is shown in Fig. 4.1. In this figure, it can be seen that the open circuit voltage (OCV) of reference case is only 0.946V instead of the ideal one, 1.23V. It is because that there exist three major types of fuel cell losses, which were mentioned in Sec. 2.2.2. In the operating voltage range from 0.6V to 0.946V, the cell's performance drops sharply because the temperature and

humidity of fuel cell do not reach balance conditions. As the stable conditions of fuel cell are achieved, the performance is mainly influenced by the ohmic loss in the operating voltage range from 0.6V to 0.4V. The current density increases with decreasing operating voltage; however, it is constrained by the concentration loss. As a consequence, the best performance is found to occur at operating voltage 0.35V to 0.4V in the following experimental results. Remind that the best performance is also affected by other factors, such as water management, ohmic resistance and etc. Table 4.3 summarizes the experimental results for the reference case at 0.35V, which can provide the best cell performance. Therefore, the following comparisons in the parametric studies are based on the results operated at 0.35V to 0.4V.

Table 4.3 The experimental results of Reference Case

Open Circuit Voltage	0.946V
The Experimental Results at Operating Voltage 0.35V	
Current Density (mA/cm^2)	599.3
Power Density (mW/cm^2)	197.8

4.2 The Influences of Current Collector Material and Conducting Area

In this part, three kinds of current collector slice materials are used. They are Cu/Au (square), Cu (square), Cu (two narrow strips), respectively, and shown in Fig. 4.2. It is known that micro PEMFC

performance is greatly affected by the resistance, whose property depends on the current collector slice material and conducting area. In the experiments, Cu (square) is chosen as the reference parameter in current collector slice material. It compares with Cu/Au (square) for material effect and with Cu (two narrow strips) for conducting area effect. If the resistance is boosted, the performance of single micro PEMFC will be lowered. Figures 4.3 (performance curve) shows the experimental results. They show that the best I-P curves for these three cases indeed occur at 0.35V to 0.4V. The comparison of the best performance is given in Table 4.4.

Table 4.4 The Best Performance for three current collector slice materials

Material \ Properties	Current Density (mA/cm^2)
Conducting Area	
Cu (two narrow strips)	136.6
Cu (square)	441.6
Material	
Cu (square)	441.6
Cu/Au (square)	534.6

In Table 4.4, it indicates that the current density of Cu/Au (square) is higher by 21.1% than that of Cu (square) at best performance. According to this, the Cu/Au (square) is chosen as the current collector slice material for the following experiments.

For the same material of Cu but with different contacting areas, the current density for Cu (two narrow strips) with conducting areas is

$0.4cm^2$, is 136.6 mA/cm^2, whereas the one for Cu (square) with conducting areas is $1cm^2$, is 441.6 mA/cm^2. It indicates that the current density of Cu (two narrow strips) is lower by 69% than that of Cu (square). However, the current density produced by Cu (square) with conducting area $1cm^2$ is about triple of that by Cu (two narrow strips) with conducting areas $0.4cm^2$, but Cu (square) with conducting area is only 2.5 times of Cu (two narrow strips) one. It indicates that the average moving distance of electrons, which is from GDL to current collector slice, can be minimized by Cu (square), as shown in Figure 4.4.

According to the present results, this work finds that both the conducting area and material of current collector slices have great influence on the performance of micro PEMFC, especially the former one.

4.3 The Influences of Gas Reheat Temperature

In the past, the performance of the large-sized PEMFC, 5cm x 5cm or 10cm x 10cm, has important relation with the gas reheat temperature, because the chemical reactions in fuel cell can be advanced by increasing reactive temperature to enhance the performance. However, it may not be true for micro PEMFC.

The resultant micro PEMFC performances shown in Figs. 4.5 (I-V curve) and 4.6 (I-P curve) indicate that the performance is not affected greatly by the gas reheat temperature. The increase of reaction temperature can indeed increases the performance; however, the enhancement is finite. Table 4.5 shows the result comparison of reheat

temperatures, 25^0C, 60^0C, and 90^0C for pure O_2 oxidizer (by flow field) at best performance.

Table 4.5 The result comparison of reheat temperatures, 25^0C, 60^0C, and 90^0C of pure O_2 oxidizer (by flow field)

Oxidizer : O_2 (by flow field)	
Reheat temperature	Current density (mA/cm^2)
25^0C	534.6
60^0C	574.2
90^0C	582.7

In Table 4.5, the current density for the reheat temperature of 90^0C is only increased by 9.1% than the one of 25^0C. Because the inside system temperature has been reached up to about 60^0C due to the heat generated by the chemical reaction, the influences on cell's performance at the reheat temperatures of 25^0C and 90^0C are expect not too much different with the conventional one.

This work carries out the same experiment for air-breathing micro fuel cell as well, and the results are shown in Figs. 4.7 (I-V curve) and 4.8 (I-P curve). They also depict that the performance is not affected greatly by the gas reheat temperature. The reason is mentioned before. Table 4.6 shows the result comparison of reheat temperatures, 25^0C, 60^0C, and 90^0C for Air-breathing fuel cell at best performance.

Table 4.6 The result comparison of reheat temperatures, 25^0C, 60^0C, and 90^0C for Air-breathing cell

Oxidizer : Air-breathing	
Reheat temperature	Current density (mA/cm2)
25^0C	136.2
60^0C	141.3
90^0C	156.4

In Table 4.6, the current density for the reheat temperature of 90^0C is only increased by 14.8% than the one of 25^0C. This experiment also reveals that increment of cell's performance is finite by increasing the gas reheats temperature.

Finally, this study suggests that the gas reheat temperature used is about 60^0C, because it can help the micro PEMFC system to reach the steady state as soon as possible.

4.4 The Influence of Bipolar Plate Open Ratio in Anode and Cathode

The open ratios of bipolar plates are designed by using different channel and rib widths under a specified depth (300μm), as shown in Table 4.7.

Table 4.7 Dimension of Flow Field Plate

Open Ratio	50%	67%	75%
Area	1.7cm×1.7cm	1.7cm×1.7cm	1.7cm×1.7cm
Flow Channel Depth	300μm		
Flow Channel Width	580μm	780μm	870μm
Rib Width	580μm	390μm	290μm

The different open ratios of bipolar plates lead to the different gas diffusion areas. MEA is not a rigid material, so the rib needs to be designed for supporting the MEA. If the bipolar plate does not have the rib to support the MEA, the resistance of fuel cell would increase and the performance would decrease. Therefore, this work carries out the study of influence of bipolar plate open ratio. In the experiments, the case of 67% open ratio is chosen as the reference one.

The performances of open ratios 50%, 67% and 75% are shown in Figure 4.9 (performance curve). They indicate that the performance is obviously increased by enhancing the open ratio. The results of the best performance are shown in Table 4.8.

Table 4.8 The best performance of three open ratios 50%, 67% and 75%

Open Ratio	Current Density (mA/cm2)
50%	551
67%	567
75%	595.4

It indicates that current density for the open ratio 75% is higher by 5% than the one of 67%. The results presents that the performance is better for open ratio 75% compared with 67%, so the former one is chosen for the following experiments: air-breathing test and long-time test. It also reveals that the open ratio has close relation with gas diffusion.

4.5 The Comparison of Three Cathode Gases With and Without Flow Channel

The pure oxygen and air are used for cathode gases separately that are fed into cell via channels by forced convection. On the other hand, an air-breathing, which air is supplied by natural convection but without cathode channel, is also designed and tested. The air is used as the cathode gas for the micro PEMFC because it is free and easy to obtain from the atmosphere. Therefore, the cost can be reduced.

Because the air contains only 21% of oxygen, this work increases the air flow rate in the test. Increasing air flow rate can avoid concentration polarization at high current density. Figure 4.10 shows the I-V curve for the air flow rate of 30sccm. It depicts that the curve becomes disorder at high current density due to concentration polarization. As the air flow rate is increased to 150sccm, the results illustrated in Fig. 4.11 show that the behavior of I-V curve is different from the one with air flow rate of 30sccm at high current density. It can be seen that the concentration polarization is improved by increasing the air flow rate at high current density, because the oxidizer can be supplied fully in cathode to enhance the reaction. The vapor quantities carried by the pure oxygen and air into the micro PEMFC are different. So these are the different test conditions for the case.

In the second part, this work makes the holistic comparisons among three oxidizer supply ways: cathode gases, which are pure O_2 and Air, separately, supplied through designed flow fields, and Air-breathing, as mentioned previously. The experimental results are shown in Figure

4.12 (performance curve). They indicate the three cases performance comparison. Table 4.9 shows the best performance comparison of three cases.

Table 4.9 The Comparison of Three Cases Cathode Gas

Three type cathode gas	Current density (mA/cm^2)
O_2 (by flow field)	599.3
Air (by flow field)	224.8
Air-breathing	193

These results indicate that current density of Air (by forced convection via flow field) is lower by 166.6% than the one of O_2 (by forced convection via flow field). Note that the oxygen quantities for both cases are the same. It is known that 78% of nitrogen N_2 is contained in air. It may occupy the part of active area to hinder O_2 from diffusing to the GDL. It is different in availability ratio between the pure oxygen O_2 and air, even if the oxygen quantities for both cases are the same. This is the reason why the case of 150sccm air flow rate let the oxygen in the air be hard to diffuse to the catalyst layer for reaction.

The resultant current density of Air-breathing (natural convection without flow channel) is lower by 14.2% than the one of Air (by forced convection via flow field). It is because the GDL diffusive capability in Air-breathing cell is lower. Therefore, if the GDL diffusive capability in the latter cell could be promoted, the differences between these two cells' performances would be reduced. The GDL diffusive capability can be improved by its material properties, such as porosity structure and hydrophilic ability. Both properties depend on the GDL material and

manufactures. In other words, the flow field plate in cathode of Air-breathing cell might not be needed.

4.6 Durability Test of micro PEMFC

A single micro PEMFC is tested for durability here. The test is carried out at a fixed operating voltage, which is 0.7V, 0.6V, 0.5V or 0.4V, for a long time (10 hours). Its purpose is to investigate whether the micro PEMFC performance is still stable after the long-time test.

Figure 4.13 shows the durability test results under four different operating voltages, which are presented by power density as a function of time. In the first three hours, the four performances appear to have a little instability because the temperature, humidity and water management of fuel cell do not reach balance conditions yet. Eventually, the system has gotten stable obviously after the three hours. It also can be observed that the performance at operating voltage 0.6V is the most stable one among the four cases, indicating that its water management is the best.

This work also makes the deviation analysis [20] for the durability test. Figure 4.13 (Power density versus Time) shows the analytical results after the three hours. It depicts that the performance deviation at fixed operating voltage 0.4V is less than ±2.2% and the one at 0.7V is less than ±1.8%, implying that the single micro PEMFC can still more or less retain a steady-state operation within 10-hour durability test. It is important for the future study and application.

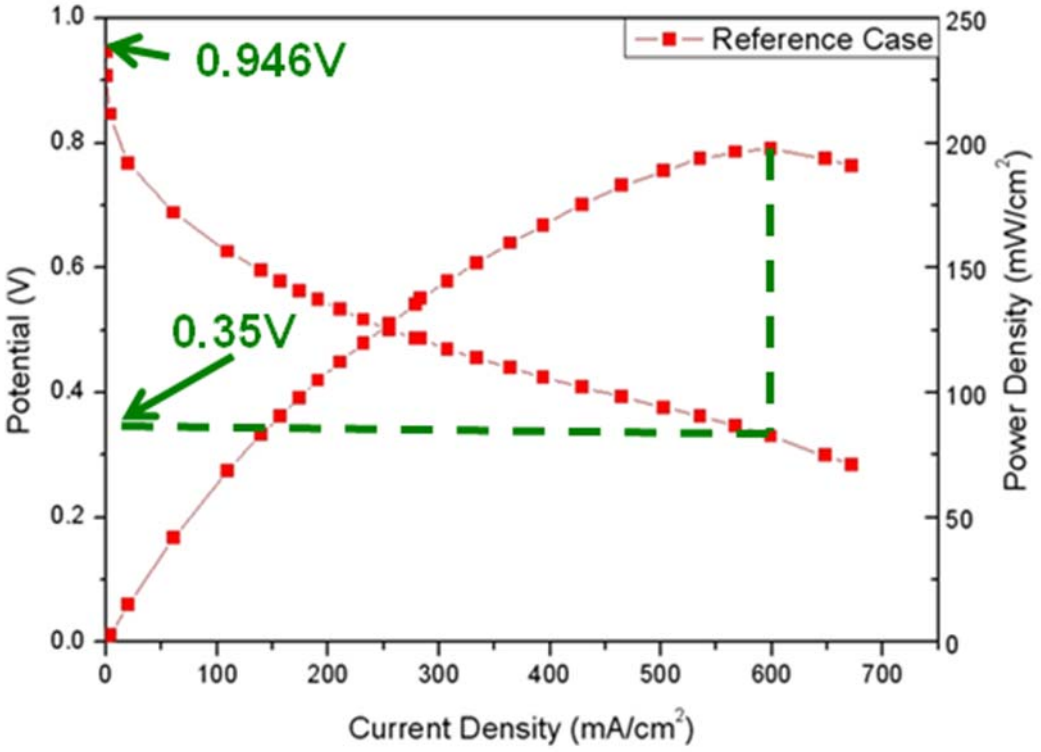

Fig. 4.1 Performance Curve of Reference Case

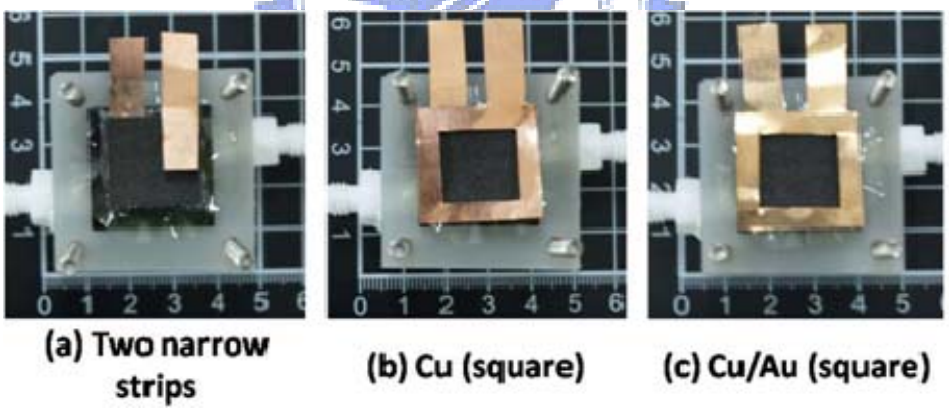

Fig. 4.2 Three Cases Current Collector slice (a) two narrow strips (b) Cu square (c) Cu/Au square

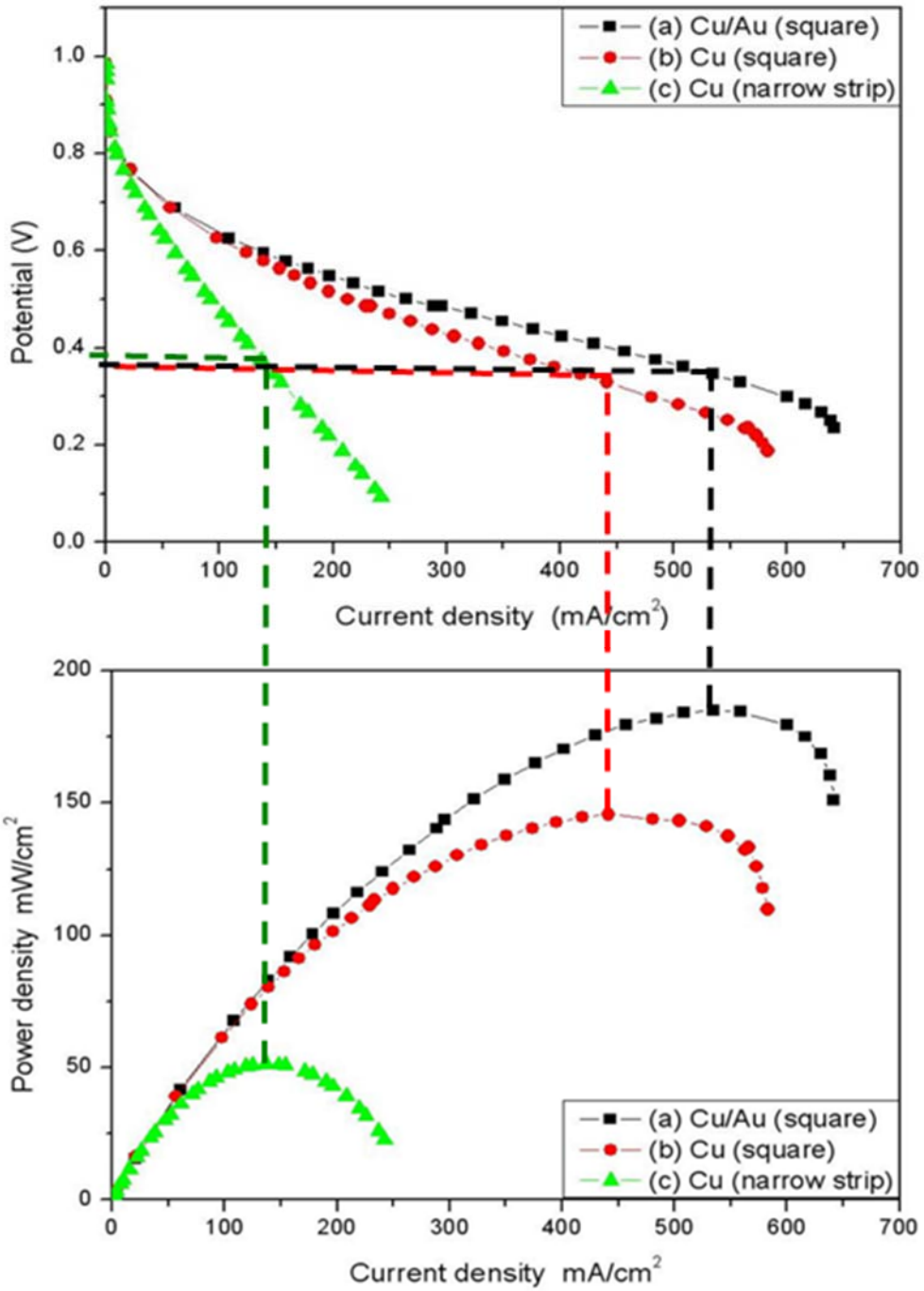

Fig. 4.3 The Performance Curve of Three Different Current Collectors

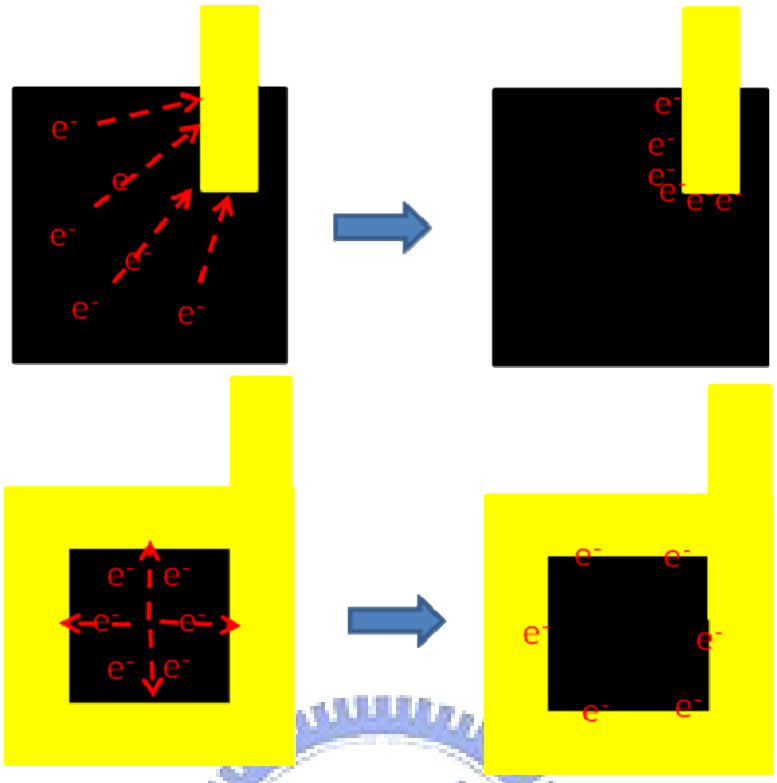

Fig. 4.4 The Average Moving Distance of Electron

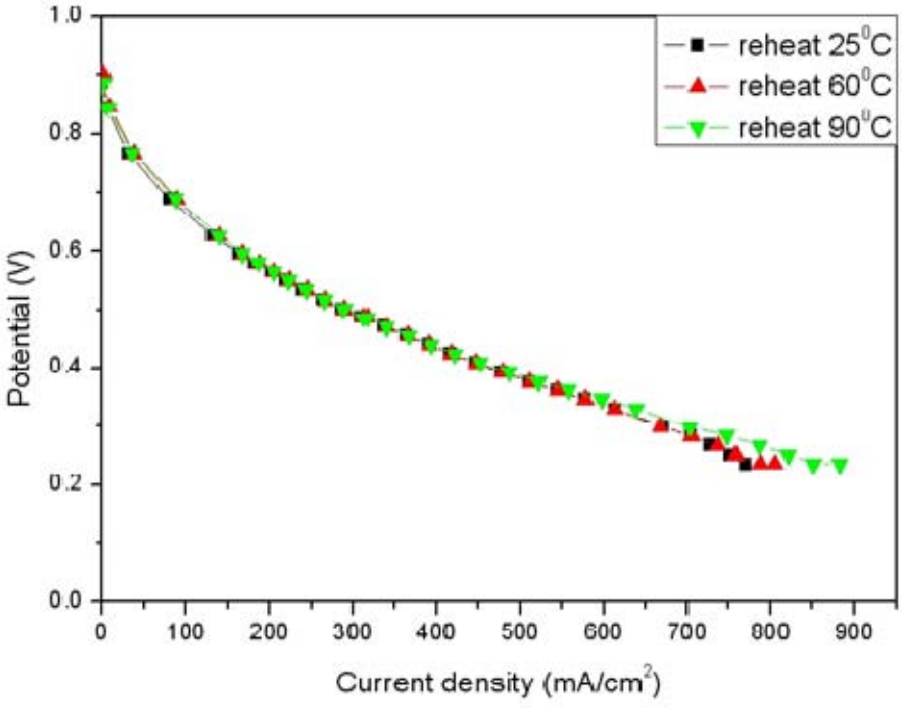

Fig. 4.5 I-V Curve of Three Reheat temperatures in O_2 (by flow field)

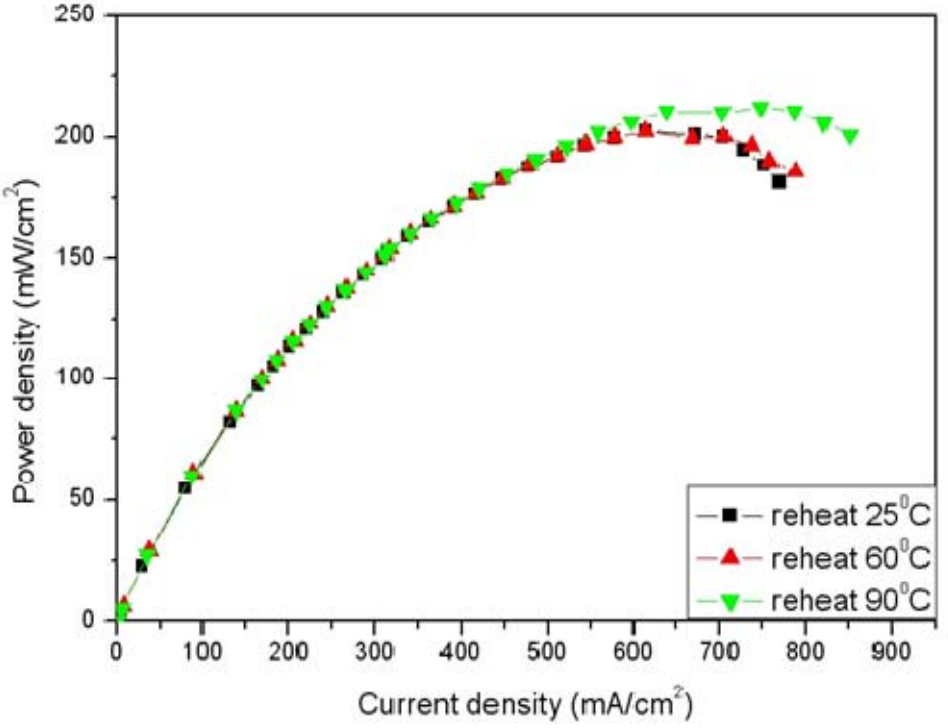

Fig. 4.6 I-P Curve of Three Reheat Temperatures in O_2 (by flow field)

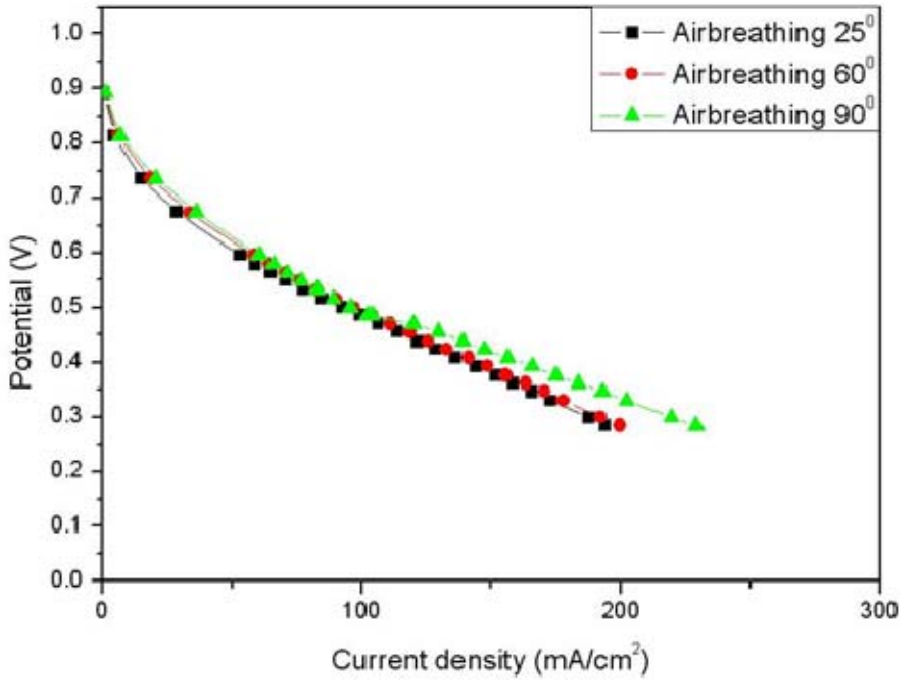

Fig. 4.7 I-V Curve of Three Reheat Temperature in Air-breathing

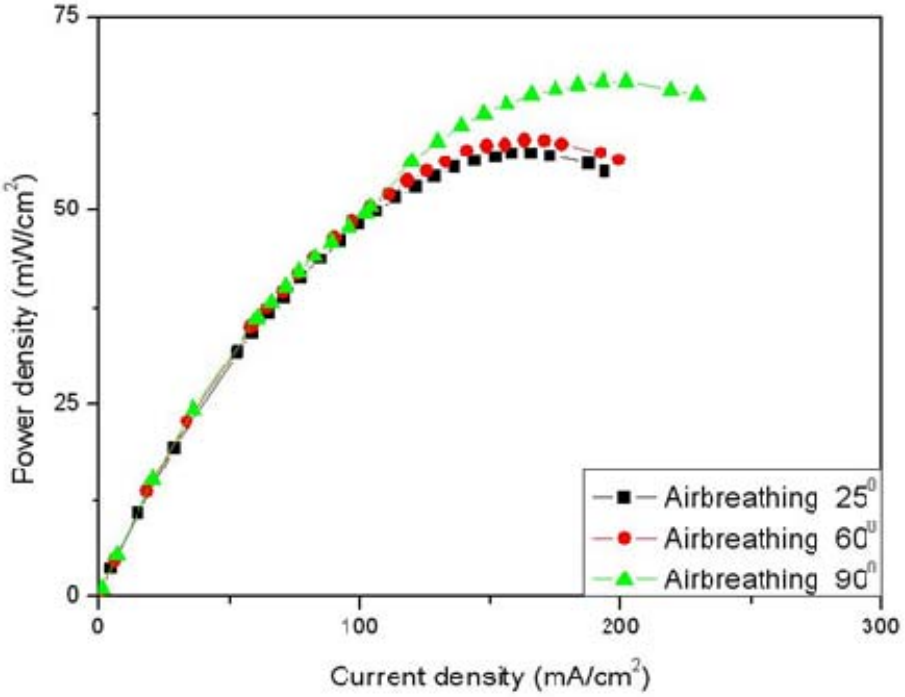

Fig. 4.8 I-P Curve of Three Reheat Temperatures in Air-breathing

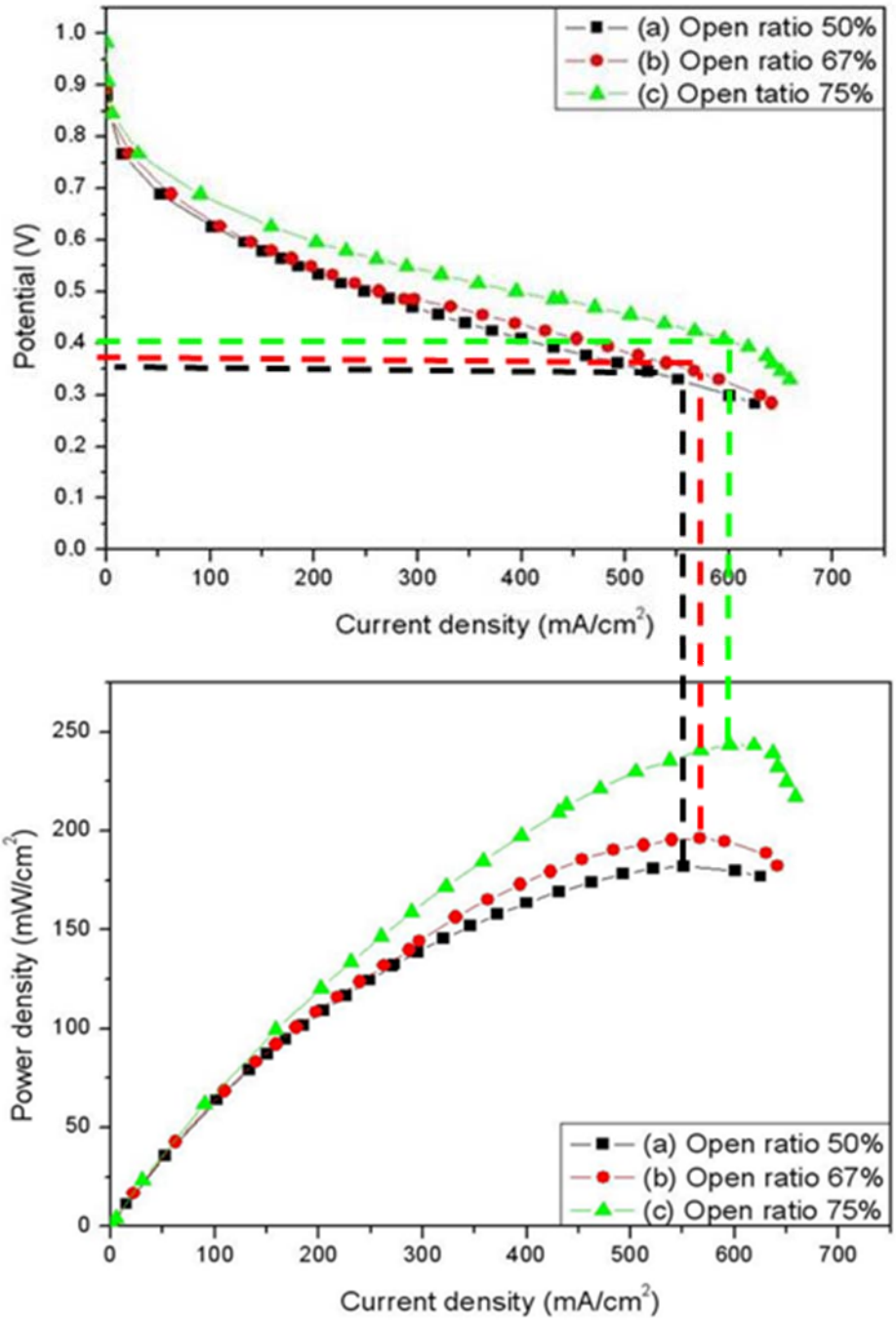

Fig. 4.9 The Performance Curve of three Open Ratios

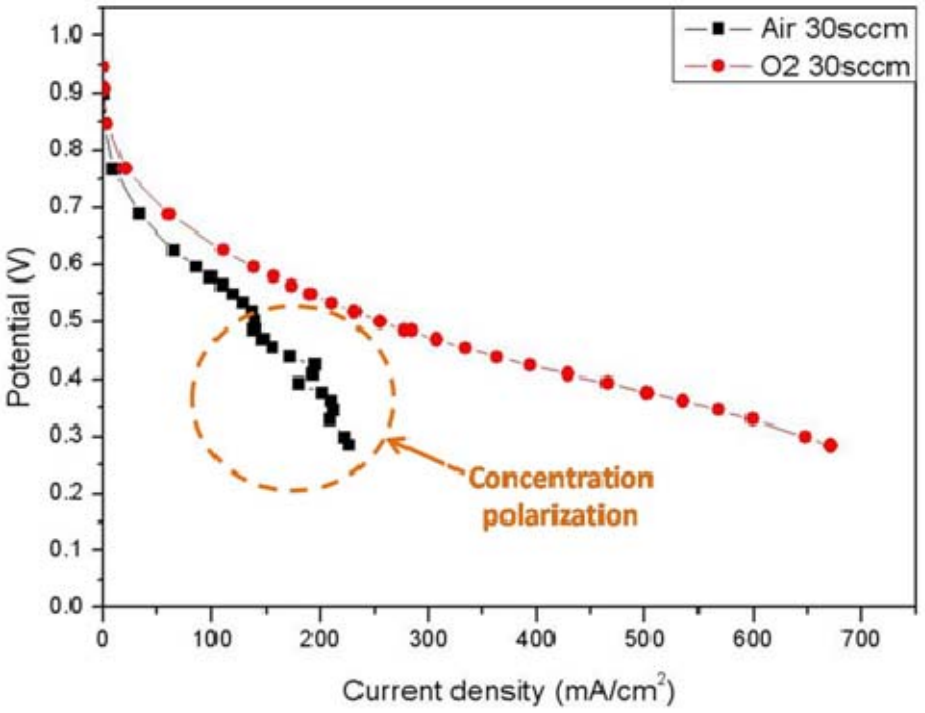

Fig. 4.10 I-V Curve at Air Flow Rate 30sccm

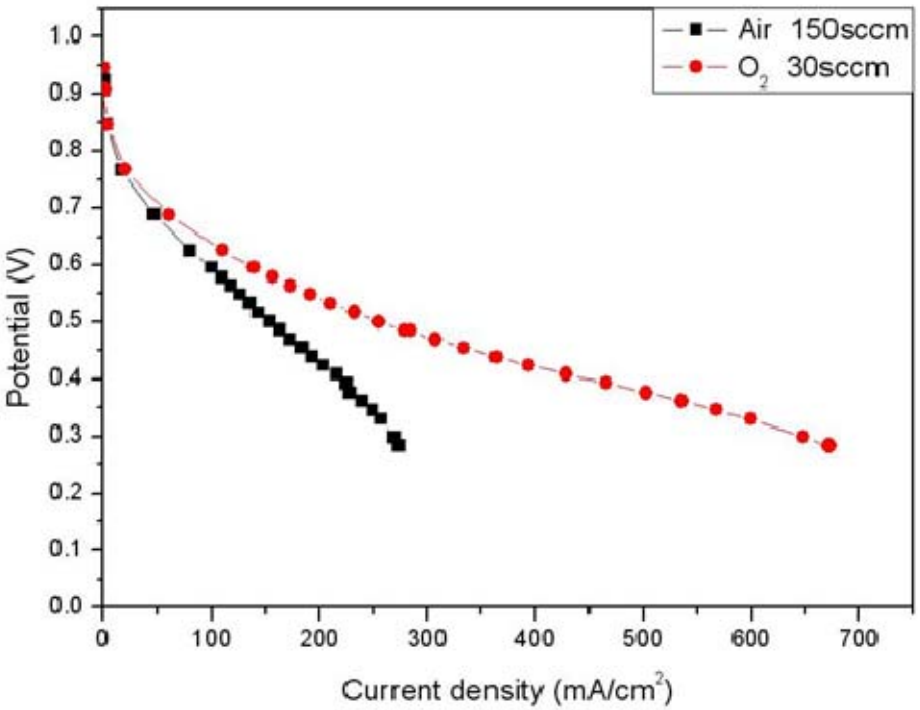

Fig.4.11 I-V Curve at Air Flow Rate 150sccm

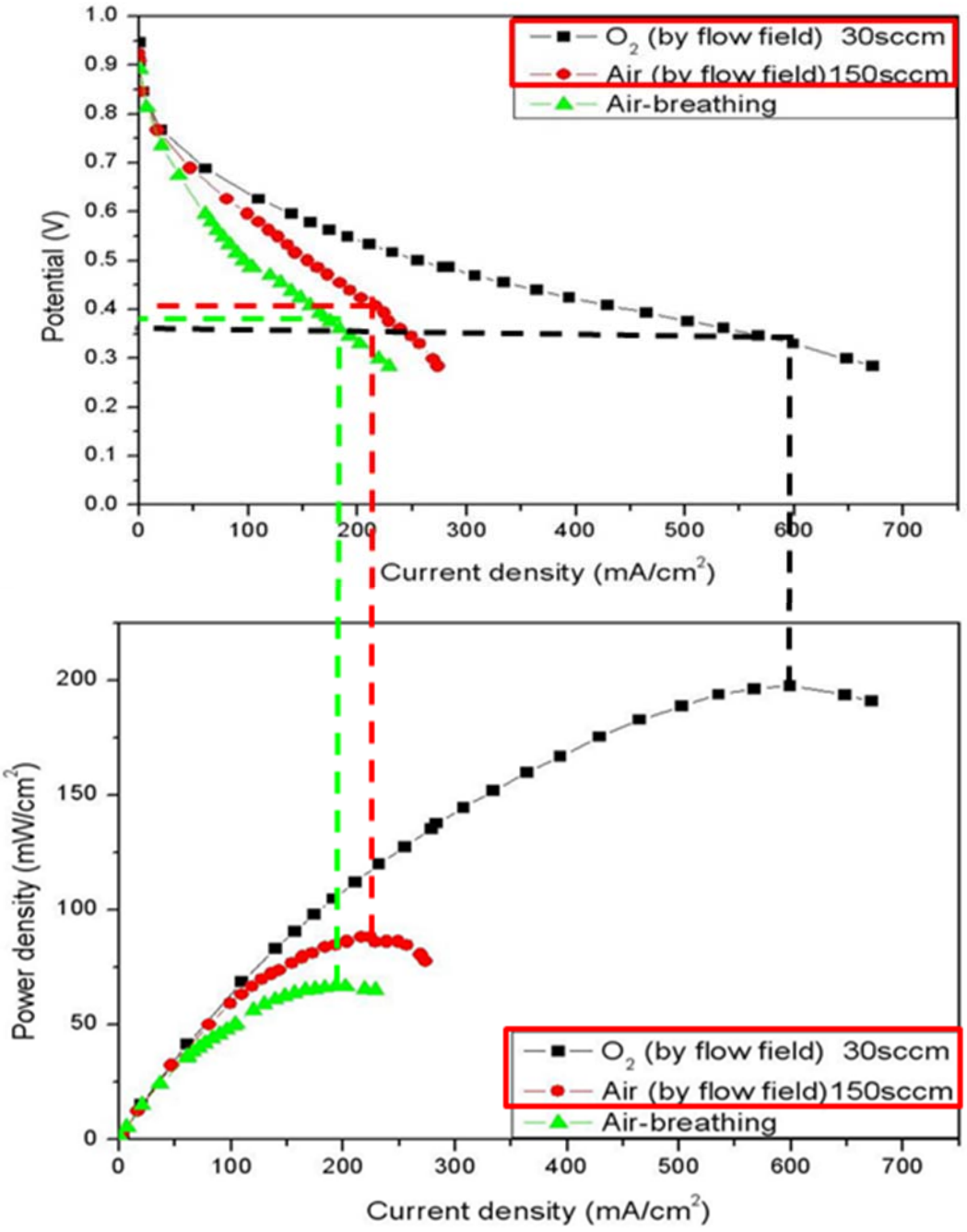

Fig. 4.12 The Performance Curve of Three Cases Cathode Gas

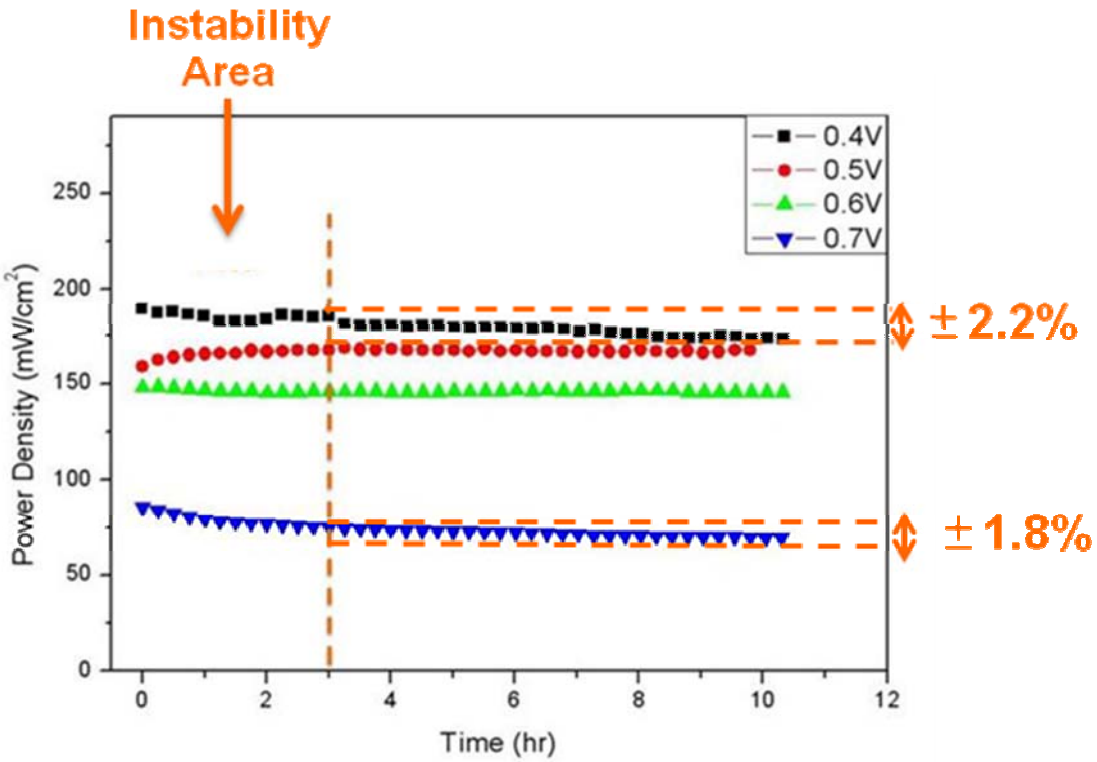

Fig.4.13 Instability Area and Deviation Analysis of Durability Test

Chapter 5

Conclusions and Recommendations

5.1 Conclusions

This work mainly studies on micro PEMFC manufactured by using MEMS technology. The study is divided into two categories; one is the parametric experimental investigation, and the other is the durability test. In experimental works, the parameters include reheat temperature, material of current collector slice, open ratio and different cathode gas, respectively.

According to above experiment results, this study can obtain the following conclusions:

1. Both the conducting area and material of current collector slices have great influence on the performance of micro PEMFC, especially the former one.
2. This experiment reveals that increment of cell's performance is finite by increasing the gas reheats temperature. Finally, this study suggests that the gas reheat temperature used is about 60^0C, because it can help the micro PEMFC system to reach the steady state as soon as possible.
3. The current density for the open ratio 75% is higher by 5% than the one of 67%. The results presents that the performance is better for open ratio 75% compared with 50% and 67%. It reveals that the open ratio has close relation with gas diffusion.
4. The concentration polarization is improved by increasing the air flow rate at high current density.

5. It is different in availability ratio between the pure oxygen O_2 and air, even if the oxygen quantities for both cases are the same.
6. The performance at operating voltage 0.6V is the most stable one among the four cases, and the performance deviation at fixed operating voltage 0.4V is less than ±2.2%.

5.2 Recommendations

This study has some lacks on the experiment. Followings are the recommendations for the future development of micro PEMFC:

1. Comparing with different material of bipolar plates, such as PDMS, and doing a series of experiments to compare with Si which is the material of bipolar plates in this study.
2. Doing the numerical simulation to investigate the distribution of water and mass transport inside the fuel cell.
3. Analyzing the impedance of micro PEMFC for durability test by A/C impedance. The increment of impedance will be investigated for analyzing which impedance of component increases.
4. Adding the conducting area between current collector slice with GDL to lower the resistance of micro PEMFC. It will increase the GDL area.
5. Thermal Imager will be used to estimate the temperature inside micro PEMFC. The tested temperature can be referred to regulate the gas reheat temperature.
6. To fix the pressure of micro PEMFC assembly. It will discuss the different pressure of assembly to investigate the experimental results.

Reference

[1] Jingrong Yu, Ping Cheng, Zhiqi Ma, Baolian Yi,"Fabrication of miniature silicon wafer fuel cells with improved performance, Journal of Power Sources, 124, pp. 40-46, May 2003.

[2] J.P. Meyers, H.L. Maynard,"Design considerations for miniaturized PEM fuel cells", Journal of Power Sources, 109, pp. 76-88 January 2002.

[3] C.-Y. Lee, C.-W. Chuang, "A novel integration approach for combining the components to minimize a micro-fuel cell", Journal of Power Sources, 172, pp.115-120, March 2007.

[4] Suhao He, Matthew M. Mench, Srinivas Tadigadapa, "Thin film temperature sensor for real-time measurement of electrolyte temperature in a polymer electrolyte fuel cell", Sensors and Actuators A, 125, pp. 170–177, May 2006.

[5] T.J McIntyre, S.W. Allison, L.C.Maxey, M.R. Cates, Progress Report (2003).

[6] Trung V. Nguyen, Ralpg E. White, "A Water and Heat Management Model for Proton-Exchange-Membrane Fuel Cells", Journal of Electrochemical Society, 140, pp. 2178-2186, August 1993.

[7] S. C. Kelly, G. A. Deluga, and W. H. Smyrl, "Miniature Fuel Cells Fabricated on Silicon Substrates", AIChE Journal, 48, pp. 1071-1082, May 2002.

[8] Keyur Shah, W. C. Shin, R. S. Besser, "Novel microfabrication approaches for directly patterning PEM fuel cell membranes", Journal of Power Sources, 123, pp. 172-181, March

2003.

[9] S.W. Cha, S. J. Lee Y. I. Park, F. B. Prinz, “Investigation of transport phenomena in micro flow channels for miniature fuel cells”, Fuel Cell Science, Engineering and Technology, FUEL CELL 2003-1709, ASME, pp.143-148, 2003.

[10] G. Q. Lu, C. Y. Wang, T. J. Yen, X. Zhang, “Development and characterization of a silicon-based micro direct methanol fuel cell”, Electrochimica Acta, 49, pp. 821-828, 2004.

[11] A. Schmitz, M. Tranitz, S. Wagner, R. Hahn, C. Hebling, “Planar self-breathing fuel cells”, Journal of Power Sources, 118, pp.162-171, 2003.

[12] A. Schmitz, S. Wagner, R. Hahn, H. Uzun, C. Hebling, “Stability of planar PEMFC in Printed Circuit Board technology”, Journal of Power Sources, 127, pp. 197-205, 2004.

[13] A. Schmitz, M. tranitz, S. Eccarius, A. Weil, C. Hebling, “Influence of cathode opening size and wetting properties of diffusion layers on the performance of air-breathing PEMFCs” Journal of Power Sources, 154, pp. 437-447, 2006.

[14] Seong Uk Jeong, Eun Ae Cho, Hyoung-Jhun Kim, Tae-Hoon Lin, In-Hwan Oh, Sung Hyun Kim, “Effects of cathode open area and relative humidity on the performance of air-breathing polymer electrolyte membrane fuel cells “, Journal of Power Sources, 158, pp. 348-353, 2006.

[15] S.W. Cha, R. O’Hayre, Y. Saito, F. B. Prinz, “The scaling behavior of flow patterns: a model investigation”, Journal

of Power Sources, 134, pp. 57-71, 2004.

[16] Jin Hyun Nam, Kyu-Jin Lee, Sangho Sohn, Charn-Jung Kim, "Multi-pass serpentine flow-fields to enhance under-rib convection in polymer electrolyte membrane fuel cells: Design and geometrical characterization", Journal of Power Sources, 188, pp. 14-23, 2009.

[17] Jason P. Kloess, Xia Wang, Joan Liu, Zhongying Shi, Laila Guessous,"Investigation of bio-inspired flow channel designs for bipolar plates in proton exchange membrane fuel cells" Journal of Power Sources, 188, pp. 132-140, 2009.

[18] Kirt R. Williams and Richard S. Muller, "Etch Rates for Micromachining Processing", Journal of Microelectromechanical System, Vol. 5, NO. 4, December 1996.

[19] Kirt R. Williams, Kishan Gupta, and Matthew Wasilik, "Etch Rates for Micromachining Processing-Part II", Journal of Microelectromechanical System, Vol. 12, NO. 6, December 2003.

[20] Shou-Shing Hsieh and Kuan-Ming Chu, "Channel and rib geometric scale effects of flowfield plates on the performance and transient thermal behavior of a micro-PEM fuel cell", Journal of Power Sources, 173, pp. 222-232, 2007.

APPENDIX A

PEMFC

The measuring uncertainty of fuel cell voltage and current are (U_V,U_I)

The minimum scale of measuring voltage in the apparatus=1mV

The voltage of the largest power V=533mV

The measuring uncertainty of voltage

$$U_v = \pm\frac{0.5}{533} = \pm 0.001$$

The minimum scale of measuring current in the apparatus=0.1mA

The current of the largest power I=2204.4mA

The measuring uncertainty of current

$$U_i = \pm\frac{0.05}{2204.4} = \pm 0.0002$$

The measuring uncertainty of fuel cell power (U_P)

$$P = I \times V$$

$$U_P = \sqrt{(U_v)^2 + (U_i)^2}$$

U_p=±0.001

Micro PEMFC

The measuring uncertainty of fuel cell voltage and current are (U_V,U_I)

The minimum scale of measuring voltage in the apparatus=1mV

The voltage of the largest power V=409mV

The measuring uncertainty of voltage

$$U_v = \pm\frac{0.5}{409} = \pm 0.001$$

The minimum scale of measuring current in the apparatus=0.1mA

The current of the largest power I=348.0*mA*

The measuring uncertainty of current

$$U_I = \pm\frac{0.05}{348.0} = \pm 0.0001$$

The measuring uncertainty of fuel cell power (U_P)

$$P = I \times V$$

$$U_P = \sqrt{(U_V)^2 + (U_I)^2}$$

$$U_p = \pm 0.001$$